Food Chemistry: X 27 (2025) 102423

Contents lists available at ScienceDirect

Food Chemistry: X

journal homepage: www.sciencedirect.com/journal/food-chemistry-x

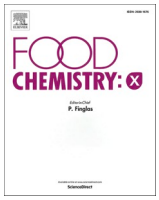

The impact of gelatinization property differences based on amylopectin structure variations on the glutinous rice flour properties and quality of Daifuku

Yu Tian [a,1], Jiaxin Li [a,1], Mengzi Nie [a], Lili Wang [a], Liya Liu [a], Fengzhong Wang [a,*], Li-Tao Tong [a,b,*]

[a] Institute of Food Science and Technology/Western Research Institute, Chinese Academy of Agricultural Sciences, Chinese Academy of Agricultural Science, Beijing 100193, China
[b] Zhongyuan Research Center, Chinese Academy of Agricultural Sciences, Xinxiang 453500, China

ARTICLE INFO

Keywords:
Daifuku
Glutinous rice
Pasting properties
Amylopectin structure

ABSTRACT

The study investigated the effects of paste viscosity for glutinous rice flour (GRF), based on differences in amylopectin structure, on the physicochemical properties of GRF and the quality of Daifuku. Ten GRF from two types (Indica variety: IGRF and Japonica variety: JGRF) were selected and the results showed the viscosity, amylopectin content, percentage of long-branched chains, enthalpy, and setback value of IGRF were significantly higher than JGRF and the Daifuku maintained an excellent appearance, which was related to higher proportion of B_2 and B_3 chain can form more double helix structure after pasting, resulting in higher hardness and compact gel network structure with improved water retention capacity. In contrast, the higher proportion of short chains in JGRF exhibited a slow retrogradation rate and formed an unstable gel network structure. All the results showed that IGRF was more suitable than JGRF to prepare Daifuku and the resulting Daifuku had better quality.

1. Introduction

Daifuku, a Japanese dessert, is prepared by glutinous rice flour (GRF) into a crust and wrapping cream within it. The dessert is spherical in shape and full, with a high moisture content in the crust, soft and viscoelastic, symbolizing the arrival of good luck, and is popular among people of all ages (Chuang & Yeh, 2006). However, the quality problems of flattened, dry, tough skin and high cracking rate of products are often found in the consumer market, which seriously hinders the sales and promotion of this product. In fact, the weak water absorption and retention capacity of GRF and the poor gel network structure is the core problem to be solved for all varieties of glutinous rice products, including Daifuku (Wang et al., 2019). Up to now, there are many methods (physical, chemical, the addition of modifier) to overcome the obstacles in the development of high-quality glutinous rice products (Rostamabadi et al., 2023). However, these methods may potentially increase the production and environmental costs, or generate undesirable flavors, making it challenging to achieve uniform and stable product quality.

From the prospective of the raw material, the property of GRF is the key factor affecting the quality of Daifuku. The manufacture of Daifuku takes advantage of the viscosity and softness of cooked glutinous rice paste, as well as the slower rate of gelatinization and retrogradation. Therefore, the gelatinization properties, especially for paste properties after gelatinization, are considerably important in the production of Daifuku, which affects the quality of the product, processability and processing conditions. In practice, suitable raw materials can produce Daifuku with good freeze-thaw stability, softness and smooth texture without relying on thickeners. Consequently, the rational selection of different varieties of GRF was anticipated to further enhance the qualities of Daifuku products by circumventing the effects of physicochemical and additives that might otherwise arise.

The properties of GRF mainly depend on its primary component, glutinous rice starch. Its gelatinization properties, particularly viscosity, are an important indicator that affects GRF-based products, which are mainly influenced by the starch structure, especially for the chain length

* Corresponding authors at: Institute of Food Science and Technology/Western Research Institute, Chinese Academy of Agricultural Sciences, Chinese Academy of Agricultural Science, Beijing 100193, China.
E-mail addresses: wangfengzhong@sina.com (F. Wang), tonglitao@caas.cn (L.-T. Tong).
[1] Co-first author.

https://doi.org/10.1016/j.fochx.2025.102423
Received 24 February 2025; Received in revised form 21 March 2025; Accepted 27 March 2025
Available online 28 March 2025

distribution of amylopectin (Jiang et al., 2024). Amylopectin contributes to the swelling of starch granules and the formation of a pasty structure. Furthermore, Li and Gong (2020) showed that the swelling and gelatinization thermodynamic properties of GRF have a highly significant correlation with the chain length distribution of amylopectin, indicating that the pasting, swelling, and disruption of glutinous rice starch granules depended on the interactions among the amylopectin chains. At present, the impact of the viscosity differences in raw GRF on the quality of Daifuku, as well as the underlying structure and influence mechanism of different glutinous rice starch behind, remains unclear. There is a lack of relevant evaluation standards and systems for producing high-quality Daifuku with GRF.

Therefore, this study aimed to select five GRF samples with different PV from each of the Indica and Japonica varieties, to establish GRF with differences in viscosity gradients, and to prepare the corresponding Daifuku. The basic component content, gelatinization properties, thermal properties, rheological properties of the GRF with different PV, and the corresponding amylopectin chain length distribution were measured. In addition, the texture, morphological structure, moisture distribution, aspect ratio and sensory characterization of the Daifuku were evaluated after freezing. In summary, this study systematically investigated the impact of GRF with different viscosity characteristics on the quality of Daifuku, providing a theoretical basis for the rapid and optimized selection of raw materials in current Daifuku production, thereby promoting the specialization and development of the GRF industry.

2. Materials and methods

2.1. Materials

This experiment used five varieties of Indica glutinous rice and five varieties of Japonica glutinous rice as the experimental materials. Five varieties of Indica glutinous rice: IR-HG (provided by Huangguoliangye Co., Ltd.); IR-JLH (provided by Jiulihu Food Co., Ltd.); IR-CJ (provided by Xiaogan Yuanfeng Grain and Oil Farmers' Professional Cooperative); IR-FJ (provided by Fangjiapuzi Green Food Co., Ltd.); IR-LXB (provided by Shaanxi Beishenghe Supply Chain Co., Ltd.). Five varieties of japonica glutinous rice: JR-YN (provided by Yunnan Lvbaokang Agricultural Technology Co., Ltd.); JR-SY (provided by Wuchang Caiqiao Rice Industry Co., Ltd.); JR-ZZH (provided by Wuchang Dida Agricultural Co., Ltd.); JR-WG (provided by Beijing Jinhe Green Source Agricultural Technology Co., Ltd.); JR-SD (provided by Jiaxiang Yongsheng Food Co., Ltd.). The white sugar used in the experiment was obtained from Hebei Gufu Food Co., Ltd. and the cream squeezed into the Daifuku comes from Shanghai Andeli Foods Co.

2.2. Preparation of GRF and Daifuku

The GRF was obtained by the semidry milling method with some modifications based on the method described by Lin et al. (2021). The glutinous rice (200 g) was pre-dried with hot air (45 °C, 60 min), followed by quantitative water absorption to obtain the desired moisture content. The water quantity was calculated based on the pre-experimental measurement of the saturation moisture content, using the following formula (1). Glutinous rice was soaked for 35 min, and after soaking, semi-dry GRF was milling using a cyclone mill (CT410, FOSS Scino (Suzhou) Co., Ltd., China). A uniform 100-mesh sieve was used for sieving to ensure consistent particle size,

$$M(g) = m \times (\omega_1 - \omega_2)/(1 - \omega_1) \quad (1)$$

In the formula:

M —— Amount of moisture necessary for saturation moisture content of glutinous rice.

m —— Glutinous rice mass before moistening.

ω_1—— Saturated moisture content of glutinous rice.

ω_2—— Moisture content of glutinous rice before moistening.

The preparation method of Daifuku was derived from Honda et al. (2023) with modifications and adaptations. The recipe for the outer layer of the Daifuku consisted of 60 g GRF, 85 g water, and 20 g white sugar, determined based on the optimal quality obtained from pre-experiments. The above ingredients were mixed thoroughly until the system was homogeneous without small lumps and then filtered through a 30-mesh baking sieve. The mixture was poured into a pan (diameter 15 cm, height 2.2 cm, bottom diameter 8.5 cm), covered with plastic wrap with a certain number of holes pierced, and then placed in a pre-heated steamer for 20 min. After cooling, knead the mixture into a dough. The entire glutinous rice dough was divided into small portions weighing 35 g each to prepare the outer layer of the Daifuku. The Daifuku crust was placed in a pre-prepared semicircular mold, filled with 1.5 g of cream, and sealed by folding diagonally. The prepared Daifuku were then placed in paper holders, and then placed in uniform square food packaging boxes for storage (specifications: inner diameter: 7 cm, height 7 cm, outer diameter: 9 cm, height 8 cm). All the prepared Daifuku were frozen at −18 °C for 24 h to simulate the state after preparation, when they entered cold chain storage awaiting distribution.

2.3. Chemical analysis

The samples were analyzed according to GB 5009.5–2016, GB 5009.6–2016 and GB 5009.4–2016 (China) for protein, fat and ash content. The total starch content was determined using a Total Starch Assay Kit (JKY/K-TSTA 07/11, Megazyme International Ltd., Wicklow, Ireland) by the American Association for Clinical Chemistry (AACC) approved method 76.13. The amylose content was determined using an Amylose/Amylopectin Assay Kit (JKY/K-AMYL 07/11, Megazyme International Ltd., Wicklow, Ireland). The summary measures of the different indicators are as follows:

2.3.1. Protein content determination (GB 5009.5–2016)

Method: Kjeldahl Method (Foss Tecator AB, Höganäs, Sweden). Procedure: Accurately weigh 1 g of the sample into a Kjeldahl flask, add concentrated sulfuric acid and a catalysto, and heat at 420 °C for 1–2 h until the solution becomes clear. Alkalinize and distill the digested solution, absorb the released ammonia in boric acid solution, and titrate with 0.1 mol/L hydrochloric acid. Calculate the nitrogen content and multiply by the protein conversion factor (typically 6.25) to determine the protein content.

2.3.2. Determination of fat content (GB 5009.6–2016)

Method: Soxhlet Extraction (FOSS Analytical, Denmark). Procedure: The dried sample is placed in a Soxhlet extractor and extracted with petroleum ether at 40–60 °C for 6–8 h. The solvent is evaporated, and the fat residue is dried at 105 °C, weighed, and calculated as fat content (%) = (fat mass / sample mass) × 100.

2.3.3. Determination of ash content (GB 5009.4–2016)

Method: Dry Ashing (Thermo Fisher Scientific, USA). Procedure: The sample is placed in a pre-weighed crucible, charred, and then ashed in a muffle furnace at 550 °C until constant weight is achieved. After cooling, the ash is weighed, and the ash content (%) is calculated as (ash mass / sample mass) × 100.

2.3.4. Determination of Total starch content

Method: AACC 76.13 Standard Method. Procedure: The sample is gelatinized with dimethyl sulfoxide (DMSO) and hydrolyzed to glucose using thermostable α-amylase and amyloglucosidase (AMG). After centrifugation, the supernatant is reacted with glucose oxidase-peroxidase (GOPOD) reagent, and the absorbance is measured at 510 nm. The glucose content is calculated from a standard curve, and the total starch content (%) is determined as (glucose content × 0.9 / sample mass) × 100.

2.3.5. Determination of amylose content

Method: Amylose/Amylopectin Assay Kit (JKY/K-AMYL 07/11, Megazyme International Ltd., Wicklow, Ireland). Procedure: The sample is mixed with 90 % dimethyl sulfoxide (DMSO) and heated in a water bath at 85 °C for 15 min to dissolve the starch. After cooling, iodine reagent (iodine-potassium iodide solution) is added and allowed to react for 10 min. The absorbance is measured at 620 nm using a spectrophotometer, and the amylose content is calculated based on a standard curve using the formula: Amylose content (%) = (amylose mass / sample mass) × 100.

2.4. Amylopectin chain length distribution of glutinous rice starch

This study employed high-performance anion-exchange chromatography (HPAEC) coupled with a CarboPac PA-200 anion-exchange column (4.0 × 250 mm; Dionex) and a pulsed amperometric detector (PAD; Dionex ICS 5000 system) to analyze the chain length distribution of amylopectin in glutinous rice starch. The sample preparation procedure was as follows: 10 mg of starch was dissolved in 5 mL of ultrapure water and heated in a boiling water bath for 60 min. Subsequently, 10 μL of 2 % sodium azide solution, 50 μL of 0.6 M sodium acetate buffer (pH 4.4), and 10 μL of 1400 U isoamylase were added, followed by incubation in a water bath at 37 °C for 24 h. After debranching, 0.5 % sodium borohydride was added for reduction over 20 h. Approximately 600 μL of the sample was dried in vacuo, dissolved in 30 μL of 1 M NaOH, and diluted with 570 μL of ultrapure water after 60 min. The HPAEC analysis conditions were as follows: flow rate of 0.4 mL/min, injection volume of 5 μL, mobile phase consisting of 0.2 M NaOH and 0.2 M NaAc, and a gradient elution program of 90:10 *V*/V at 0 min, 90:10 V/V at 10 min, 40:60 V/V at 30 min, 40:60 V/V at 50 min, 90:10 V/V at 50.1 min, and 90:10 V/V at 60 min. Data were acquired using the ICS5000 system and processed with Chromeleon 7.2 CDS software, with quantitative results exported in Excel format (Zhou et al., 2015).

2.5. Powder X-ray diffraction (XRD)

An X-ray powder diffractometer (Bruker D8 Advance, Germany) was used to analyze the crystallization characteristics of rice flour. All samples were equilibrated in a sealed container containing saturated lithium chloride solution (30 °C) to reach a similar moisture content (~10 %) prior to XRD analysis. The X-ray source was Cu-Kα radiation (λ = 0.1542 nm) with a scanning step width of 0.02° at 40 kV and 40 mA. The results were obtained by scanning from 5° to 45° (2θ, the angle of diffraction) at a rate of 10°/min. The relative crystallinity was calculated by the MDI Jade 6.0 software (Materials Data, Inc., USA). This method was adapted from Chi et al. (2018) with slight modifications.

2.6. FTIR

Samples of GRF (2 mg) and dried KBr powder (200 mg) were thoroughly mixed using a grinder. The infrared (IR) spectra of starches were measured using a Tensor 27 FTIR spectrometer (Bruker, Germany) equipped with a DLATGS detector. The spectra were scanned in the range of 4000–400 cm^{-1}, with an accumulation of 64 scans and a resolution of 4 cm^{-1}. All spectra were automatically baseline-corrected in the range of 1200 and 800 cm^{-1} by OMNIC 8.0 before being deconvoluted with a half-band width of 19 cm^{-1} and an enhancement factor of 1.9. The ratio of absorbance at 1047/1022 cm^{-1} was used to estimate the short-range ordered structure of starch. The measurements of each sample were conducted in triplicate (Gong et al., 2023).

2.7. Pasting properties

The gelatinization characteristics of the GRF were determined using a Rapid Visco Analyzer (RVA-TecMaster, Perten Instruments, NSW, Australia). Based on the initial moisture content, the RVA software was used to make adjustments. The GRF and deionized water, were weighed and added to an aluminum RVA canister, achieving a total weight of 28.00 g under a humidity benchmark based on 14 %. The experimental parameters were slightly modified as described in Geng et al. (2020).

2.8. Thermodynamic properties

The thermal properties of different varieties of GRF were measured using a differential scanning calorimeter (DSC 8000, Perkin Elmer, Norwalk, CT, USA) according to the method described by Boulemkahel et al. (2021). A mixture of 3 mg GRF (dry basis) and 10 μL distilled water was added to an aluminum box, sealed, and equilibrated at 4 °C for 24 h. Measurements were taken at the end of equilibration. The program was heated from 30 °C to 100 °C at a rate of 10 °C/min. The blank control was a sealed empty aluminum box. The onset temperature (To), peak temperature (Tp), conclusion temperature (Tc), and enthalpy change value (ΔH) were calculated using DSC Instruments software (Perkin-Elmer, Norwalk, CT, USA).

2.9. In vitro starch digestibility

This method was adapted from You et al. (2014) with slight modifications. Brief Procedure: Accurately weigh 50 mg of GRF sample and disperse it in 2 mL of distilled water. Heat the mixture in a boiling water bath for 30 min. After gelatinization, cool the sample to 37 °C. First, add 7 glass beads and 20 mL of sodium acetate buffer (pH 5.2) into a 50 mL centrifuge tube, and incubate in a water bath at 37 °C (MTH-100, Hangzhou, Miou Instrument Co., Ltd.) for 20 min. Then, transfer 300 μL of the mixture into a 5 mL centrifuge tube, add 3 mL of anhydrous ethanol, vortex thoroughly, and centrifuge at 10,000 *g* for 5 min. Collect the supernatant as the 0-min digestion sample. Next, add 2 mL of mixed enzyme solution to the reaction system, and at 20, 120, and 180 min, take 0.3 mL of the digestion mixture, add 3 mL of anhydrous ethanol, mix well, and centrifuge at 10,000 *g* for 5 min.

Transfer the supernatants from the centrifugation at different time points into clean centrifuge tubes. Take 0.1 mL of each supernatant and add 3 mL of GOPOD reagent. Incubate the mixture in a water bath at 50 °C for 20 min. Then, transfer 200 μL of the reaction mixture to a microplate and measure the absorbance at 520 nm. The mixed enzyme solution is prepared as follows: dissolve 2 portions of 4.5 g pancreatin in 2 portions of 40 mL deionized water, vortex thoroughly, and incubate in a water bath at 37 °C for 10 min. Finally, centrifuge at 5000 *g* for 10 min.

2.10. Rheological properties

The rheological properties of Daifuku dough formed after steaming were determined according to He et al. (2023) with minor modifications. The samples were measured in a 40 mm diameter plate with 1 mm gap. After 0.01–10 % strain scanning test on Daifuku dough by Rheometer (Physica MCR 301, Anton Paar GmbH, Austria), the oscillation frequency experiment (0.1–10 Hz) was carried out in the linear viscoelastic region with 0.1 % target strain. Recording the elastic modulus (G'), viscous modulus (G") and loss tangent (tan δ) of the Daifuku dough.

2.11. Microstructure

The microstructure of frozen Daifuku crust was determined according to the method of Wang et al. (2019) with some modifications. All the samples were observed using scanning electron microscopy (SEM, Hitachi S-570, Hitachi, Co., Ltd., Tokyo, Japan) under an acceleration voltage of 10 kV, and at magnifications of 500× after sputter-coating with gold. The frozen Daifuku were thawed for 30 min at 5 °C, and cut in half to observe the cross-sectional appearance, the length, width, and height were measured.

2.12. Whiteness

The color of the outer layer of Daifuku was measured using a spectrophotometer. It was expressed using the L* (lightness), a* (redness), and b* (yellowness) values. The whiteness index was calculated as following formula (2) (Lin et al., 2021):

$$\text{Whiteness} = 100 - \left[(100 - L)^2 + a^2 + b^2\right]^{0.5} \quad (2)$$

2.13. Textural properties

The textural properties of cooked Daifuku obtained in section 2.2 were determined in texture profile analysis (TPA) mode using a TAXT 2i/5 texture analyzer (Stable Micro System Ltd., Godalming, England) and a P/36R probe, following a reported method with some modifications (Wang et al., 2019). Measurements were performed on cooked crusts after equilibration at 4 °C for 20 min. The parameters were as follows: descent rate of 2.0 mm/s, test rate of 1.0 mm/s, rise rate of 1.0 mm/s, trigger force of 5.0 g, and compression strain of 50 %.

2.14. Low-field nuclear magnetic resonance (LF-NMR)

According to the method of He et al. (2020) with some modifications. An LF-NMR analyzing and imaging system (NMI20-030H-I, Niumag Electronic Technology Co., Ltd., Shanghai China) was used to determine the water states of the Daifuku crust. The transverse relaxation time (T2) of Daifuku was determined using the CarrPurcell-Meiboom-Gill (CPMG) sequence. The parameters were set as follows: spectrometer frequency (SF) = 21 MHz, time of echo (TE) = 0.1 ms, echo count (NECH) = 2000, and the number of scans (NS) = 64. Assays were performed in triplicate.

2.15. Sensory evaluation and ethical compliance statement

Daifuku's sensory evaluation was completed by 30 general consumer volunteers (70 % female and 30 % male) between the ages of 20 and 50 using a 9-point favorability scale (1-extremely unpleasant and 9-extremely pleasant). They knew about sensory analysis of food, but they were not specially trained to judge Daifuku's quality. The analysis was performed using the rules of previous studies (Chochkov et al., 2022) with slight modification. The volunteers were requested to evaluate 7 parameters the appearance, apparent color, viscoelasticity, aroma, chewiness, taste and acceptability. The analysis was based on the average of the sensory evaluations. The sensory analysis experiments conducted in this study strictly adhered to local ethical guidelines and have been formally approved by the Ethics Committee of *IFST-CAAS* (Institute of Food Science and Technology, Chinese Academy of Agricultural Sciences). The authors solemnly declare that the rights and privacy of all participants were fully protected throughout the implementation of the research. Specific measures included ensuring voluntary participation, providing comprehensive disclosure of research requirements and potential risks, obtaining written consent from participants, prohibiting the disclosure of participant data without explicit authorization, and allowing participants to withdraw from the study at any time. A detailed statement of consent for participation in the sensory evaluation research has been submitted as supplementary material.

2.16. Statistical analysis

Significant differences between samples were determined by one way analysis of variance (ANOVA) with Duncan's test ($P < 0.05$) using the SPSS software 26.0 (SPSS Inc., Chicago, IL, USA). The data were expressed as means ± standard deviation (SD). Origin 2021 software was used for charting and principal component analysis (PCA).

3. Results and discussion

3.1. Chemical composition of GRF

The basic components of 10 varieties of GRF were shown in Table 1. Different varieties of glutinous rice differed in terms of amylose, protein, ash and lipid content. In this experiment, the average contents of basic components in these two types of GRF were determined separately. The average total starch content of IGRF (85.73 %) was higher than that of JGRF (82.56 %). Among them, the average content of amylose was 5.67 % and 4.57 % in IGRF and JGRF, respectively, and the protein content (7.23 %) and ash content (0.64 %) of JGRF were higher than those of IGRF (6.73 % and 0.24 %, respectively). These differences were related to the varieties, growth conditions and environment. It is noteworthy that the lipid content of IGRF was considerably lower than that of JGRF, with average contents of 0.39 % and 1.70 %, respectively.

3.2. Amylopectin chain length distribution of glutinous rice starch

Normalized chromatograms of the branch chain length distribution of amylopectin are presented in Fig. 1, while the amylopectin chain length distribution of the ten debranched GRF starch samples is summarized in Table 2, demonstrating a degree of polymerization (DP) range of 6 to 76. According to the statistics in Table 2, there were significant differences in the amylopectin chain length distribution between IGRF and JGRF. The proportion of A_{fp} chains (DP 6–8) in JGRF was higher than that of IGRF as a whole, with JR-SY having the highest proportion of 5.75 %, followed by JR-YN with a proportion of 5.66 %, and IR-LXB with the lowest proportion of 2.67 %. A_{fp} is the shortest chain in amylopectin, which was too short to form a double helix structure and cannot participate in the formation of crystalline lamellae in starch granules, so the amount of A_{fp} chain was negatively correlated with ΔH (Table 3), pasting temperature and PV, the same result was found in the study of Gayin et al. (2016). In contrast, the amount of B_2 and B_3 chains (DP > 25) was positively correlated with the ΔH. The proportion of B_2 and B_3 of IR-LXB was 25.32 %, which was the highest among IGRF and the B_2 and B_3 proportion of JR-SD was 23.30 %, which was the highest among JGRF ($P < 0.05$). The average DP of IGRF was higher than that of JGRF. It was commonly accepted that the average DP of amylopectin was another crucial factor in determining the gelatinization properties of starch (Li et al., 2022). In fact, starch chains with higher average DP are more likely to form stable double helix structures, requiring more heat for gelatinization and having higher ΔH. Long chain starch with longer average DP can form more cross-linking points, making it more complex to interweave during gelatinization, thereby increasing starch viscosity. This was consistent with the fact that IGRF has higher ΔH and PV than JGRF. Furthermore, the retrogradation of amylopectin was positively correlated with the proportion of long chains, and longer chain would facilitate the formation of increasingly ordered double-helix structures, which was similar to the investigation in wheat starch (Huang et al., 2022). This phenomenon also indicated that IGRF might exhibit a higher degree of retrogradation than JGRF during a longer storage period, which may ultimately lead to a higher product hardness and make the product maintain a more stable appearance.

3.3. Crystalline structure of starch

The long-range ordered nature of crystals can be characterized by their relative crystallinity (RC). The XRD patterns and RC of the GRF samples are shown in Fig. 3A. It can be observed that the RF exhibits a typical A-type crystalline structure, with strong diffraction peaks at 15°, 17°, 18°, and 23° (2θ), which is consistent with the findings reported by Zhang et al. (2022). The relative crystallinity calculated from the XRD patterns shows significant differences among the ten types of GRF, ranging from 18.50 % for IR-LXB to 13.53 % for JR-YN (Fig. 2). Notably,

Table 1
Approximate composition of different types of GRF. Means values ± standard deviation, $n = 3$. Different superscript letters in the same row indicate significant differences at $P < 0.05$.

	IGRF					Average content	JGRF					Average content
	IR-LXB	IR-FJ	IR-CJ	IR-JLH	IR-HG		JR-SD	JR-WG	JR-ZZH	JR-SY	JR-YN	
Total starch (%)	85.08 ± 0.16^{d}	85.52 ± 0.23^{c}	85.75 ± 0.14^{b}	85.93 ± 0.25^{b}	86.35 ± 0.53^{a}	85.73 ± 0.29^{b}	81.19 ± 0.22^{j}	83.36 ± 0.16^{f}	84.34 ± 0.06^{e}	81.85 ± 0.09^{i}	82.08 ± 0.04^{h}	82.56 ± 0.03^{g}
Amylose content (%)	6.12 ± 0.12^{a}	6.03 ± 0.04^{b}	5.88 ± 0.19^{c}	5.32 ± 0.20^{e}	5.02 ± 0.63^{f}	5.67 ± 0.17^{d}	4.44 ± 0.20^{h}	4.32 ± 0.01^{i}	4.14 ± 0.09^{j}	3.68 ± 0.09^{k}	3.28 ± 0.02^{l}	4.57 ± 0.25^{g}
Amylopectin content (%)	93.88 ± 0.20^{j}	93.97 ± 0.93^{hi}	94.12 ± 0.72^{h}	94.68 ± 0.09^{g}	94.98 ± 0.09^{f}	94.33 ± 0.42^{e}	95.56 ± 0.12^{e}	95.68 ± 0.29^{de}	95.86 ± 0.16^{d}	96.32 ± 0.70^{b}	96.72 ± 0.11^{a}	96.03 ± 0.34^{c}
Protein (%)	7.02 ± 0.05^{e}	7.00 ± 0.03^{ef}	6.94 ± 0.06^{g}	6.49 ± 0.05^{i}	6.04 ± 0.04^{j}	6.73 ± 0.04^{h}	7.36 ± 0.04^{a}	7.20 ± 0.03^{cd}	7.02 ± 0.02^{fg}	7.26 ± 0.03^{bc}	7.30 ± 0.01^{ab}	7.23 ± 0.02^{bc}
Lipid (%)	0.35 ± 0.02^{f}	0.34 ± 0.00^{f}	0.49 ± 0.22^{d}	0.38 ± 0.01^{e}	0.41 ± 0.01^{e}	0.39 ± 0.08^{e}	1.92 ± 0.28^{a}	2.04 ± 0.05^{a}	1.97 ± 0.19^{a}	1.93 ± 0.11^{a}	0.66 ± 0.08^{c}	1.70 ± 0.12^{b}
Ash (%)	0.28 ± 0.02^{e}	0.16 ± 0.06^{h}	0.27 ± 0.12^{ef}	0.23 ± 0.06^{gg}	0.25 ± 0.01^{f}	0.24 ± 0.05^{f}	0.66 ± 0.14^{c}	0.75 ± 0.07^{b}	0.77 ± 0.11^{a}	0.77 ± 0.00^{bc}	0.27 ± 0.02^{e}	0.64 ± 0.05^{d}

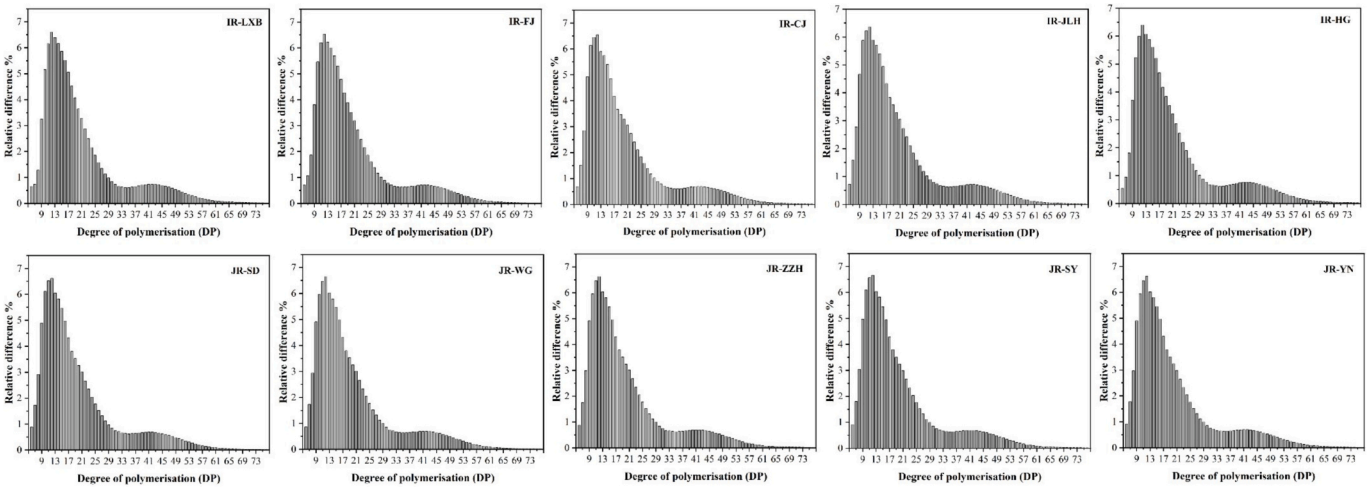

Fig. 1. Distribution of branched-chain starch chain lengths of different GRF.

Table 2
Branch chain length distribution of starch extracted from different varieties of GRF.

	IGRF					JGRF				
	IR-LXB (%)	IR-FJ (%)	IR-CJ (%)	IR-JLH (%)	IR-HG (%)	JR-SD (%)	JR-WG (%)	JR-ZZH (%)	JR-SY (%)	JR-YN (%)
A_{fp} (DP6–8)	2.67 ± 0.02^{h}	3.30 ± 0.02^{g}	3.64 ± 0.01^{f}	5.04 ± 0.01^{e}	5.06 ± 0.02^{e}	5.53 ± 0.01^{d}	5.54 ± 0.01^{d}	5.62 ± 0.03^{c}	5.75 ± 0.01^{a}	5.66 ± 0.03^{b}
$A_{crystal}$ (DP9–12)	21.17 ± 0.01^{h}	22.00 ± 0.02^{f}	24.06 ± 0.02^{c}	23.13 ± 0.03^{e}	21.32 ± 0.02^{g}	24.16 ± 0.01^{b}	23.99 ± 0.01^{cd}	23.97 ± 0.05^{d}	24.29 ± 0.01^{a}	23.94 ± 0.04^{d}
A(DP $\leq$ 12)	23.84 ± 0.01^{d}	25.64 ± 0.01^{c}	29.10 ± 0.02^{b}	28.19 ± 0.2^{b}	24.61 ± 0.02^{c}	29.69 ± 0.01^{a}	29.53 ± 0.01^{a}	29.59 ± 0.04^{a}	30.04 ± 0.04^{a}	29.60 ± 0.04^{a}
B_1(DP13–24)	52.04 ± 0.01^{a}	50.34 ± 0.01^{b}	49.72 ± 0.02^{b}	47.24 ± 0.04^{c}	46.82 ± 0.02^{c}	47.27 ± 0.02^{c}	47.19 ± 0.01^{c}	47.17 ± 0.04^{c}	47.08 ± 0.04^{c}	47.05 ± 0.01^{c}
B_2(DP25–36)	11.61 ± 0.01^{d}	11.94 ± 0.01^{bc}	11.89 ± 0.02^{c}	12.03 ± 0.02^{a}	11.95 ± 0.02^{b}	11.58 ± 0.01^{d}	11.62 ± 0.01^{d}	11.58 ± 0.04^{d}	11.58 ± 0.01^{d}	11.52 ± 0.04^{d}
B_3(DP $\geq$ 37)	13.71 ± 0.02^{a}	12.53 ± 0.02^{b}	12.51 ± 0.01^{b}	12.18 ± 0.02^{c}	12.08 ± 0.01^{d}	11.72 ± 0.04^{e}	11.61 ± 0.04^{ef}	11.61 ± 0.01^{f}	11.46 ± 0.01^{g}	11.33 ± 0.01^{h}
B_2 and B_3 (DP >25)	25.32 ± 0.03^{a}	24.47 ± 0.03^{b}	24.40 ± 0.03^{c}	24.21 ± 0.04^{d}	24.03 ± 0.03^{e}	23.30 ± 0.05^{f}	23.23 ± 0.05^{g}	23.19 ± 0.05^{g}	23.04 ± 0.02^{h}	22.85 ± 0.05^{i}
Average DP	21.18 ± 0.02^{a}	20.75 ± 0.01^{b}	20.49 ± 0.02^{c}	20.46 ± 0.02^{c}	20.27 ± 0.01^{d}	19.99 ± 0.04^{e}	19.89 ± 0.01^{f}	19.97 ± 0.01^{e}	19.92 ± 0.04^{e}	19.81 ± 0.01^{g}

Means values ± standard deviation, n = 3. Different superscript letters in the same row indicate significant differences at $P < 0.05$.

the relative crystallinity of IGRF is generally higher than that of JGRF. The decrease in crystallinity indicates an increase in the disorder of the crystalline structure, leading to a reduction in the energy required to melt the crystals during the heating and gelatinization process. This is consistent with the thermal properties of the GRF (Table 2). Studies have shown that the proportion of short chains (DP < 10 and DP 10–13) in amylopectin plays a crucial role in the formation of crystallinity, with a higher proportion resulting in lower starch crystallinity. This is because the presence of short chains reduces the stability of the double helix structure. On the other hand, Miao et al. (2015) suggested that a higher

Table 3
Pasting and thermal properties of various GRF.

	IGRF					JGRF				
	IR-LXB	IR-FJ	IR-CJ	IR-JLH	IR-HG	JR-SD	JR-WG	JR-ZZH	JR-SY	JR-YN
Pasting properties										
PV (cP)	4508.12 ± 5.66[a]	3895.63 ± 9.19[b]	3753.82 ± 3.54[c]	3577.53 ± 4.25[d]	3458.68 ± 10.60[e]	3137.42 ± 6.60[f]	2987.77 ± 6.36[g]	2777.38 ± 5.32[h]	2626.14 ± 6.36[i]	2521.75 ± 8.49[j]
TV (cP)	2133.56 ± 4.24[a]	1978.82 ± 3.54[b]	1724.42 ± 5.65[c]	1700.27 ± 7.07[d]	1603.33 ± 4.95[e]	1194.58 ± 9.19[f]	1058.88 ± 8.48[g]	938.96 ± 4.95[h]	828.07 ± 8.49[i]	689.44 ± 2.83[j]
BD (cP)	2392.68 ± 7.78[a]	2033.55 ± 2.83[b]	1990.32 ± 4.24[c]	1930.87 ± 3.54[d]	1878.62 ± 5.66[e]	1983.30 ± 5.66[c]	1932.87 ± 5.62[d]	1847.58 ± 10.60[f]	1830.44 ± 9.19[g]	1811.57 ± 8.49[h]
FV (cP)	2624.72 ± 4.24[a]	2454.53 ± 6.02[b]	2222.37 ± 2.72[c]	2198.62 ± 5.13[c]	2379.22 ± 5.66[b]	1465.71 ± 6.61[d]	1331.48 ± 8.49[e]	1194.36 ± 5.12f	1070.82 ± 5.46 g	956.88 ± 4.33 h
SB (cP)	452.21 ± 2.83[a]	421.52 ± 4.95[a]	398.50 ± 3.54[a]	364.34 ± 2.83[a]	355.46 ± 4.90[a]	298.56 ± 5.26[b]	277.61 ± 5.66[c]	258.80 ± 2.83[d]	237.66 ± 5.66[e]	229.86 ± 3.77[f]
PT (°C)	81.11 ± 0.15[a]	78.22 ± 0.02[b]	77.12 ± 0.03[c]	75.67 ± 0.04[d]	73.83 ± 0.03[e]	70.13 ± 0.04[f]	69.71 ± 0.01[g]	69.44 ± 0.06[h]	69.25 ± 0.02[i]	68.81 ± 0.01[j]
Thermal properties										
T_o (°C)	76.18 ± 0.05[a]	75.94 ± 0.08[b]	66.56 ± 0.08[c]	66.17 ± 0.05[d]	65.97 ± 0.02[e]	62.30 ± 0.06[f]	61.21 ± 0.02[g]	60.89 ± 0.05[h]	60.59 ± 0.04[i]	60.42 ± 0.02[j]
Tp (°C)	80.43 ± 0.05[a]	80.18 ± 0.05[b]	71.49 ± 0.04[c]	70.87 ± 0.03[d]	70.57 ± 0.05[e]	68.23 ± 0.05[f]	67.88 ± 0.04[g]	67.77 ± 0.06[gh]	67.74 ± 0.04[h]	67.29 ± 0.05[i]
Tc (°C)	84.72 ± 0.09[a]	84.00 ± 0.04[b]	78.58 ± 0.05[c]	75.85 ± 0.06[d]	75.53 ± 0.05[e]	75.06 ± 0.07[f]	74.83 ± 0.04[g]	74.68 ± 0.05[g]	74.41 ± 0.04[h]	74.35 ± 0.07[h]
ΔH(J/g)	9.11 ± 0.06[a]	8.48 ± 0.08[b]	8.19 ± 0.04[c]	7.58 ± 0.06[d]	7.42 ± 0.07[d]	7.11 ± 0.04[e]	6.92 ± 0.05[f]	6.64 ± 0.10[g]	6.46 ± 0.05[h]	6.29 ± 0.11[h]
FTIR										
R1047/1022	0.7155 ± 0.0077[a]	0.7086 ± 0.0085[b]	0.7055 ± 0.0063[c]	0.7011 ± 0.0027[d]	0.6992 ± 0.0062[e]	0.6873 ± 0.0014[f]	0.6845 ± 0.0036[g]	0.6802 ± 0.0029[h]	0.6770 ± 0.0084[i]	0.6743 ± 0.0049[j]
R1022/995	0.5376 ± 0.0025[a]	0.5219 ± 0.0043[b]	0.5210 ± 0.0161[c]	0.5166 ± 0.0032[d]	0.5123 ± 0.0056[e]	0.5101 ± 0.0017[f]	0.5089 ± 0.0027[g]	0.5072 ± 0.0049[h]	0.5060 ± 0.0019[i]	0.5047 ± 0.0033[j]

[a] Means values ± standard deviation, $n = 3$. Different superscript letters in the same row indicate significant differences at $P < 0.05$.
[b] PV, peak viscosity; TV, trough viscosity; BD, breakdown viscosity; FV, final viscosity; SB, setback viscosity; PT, pasting temperature; To, onset temperature; Tp, peak temperature; Tc, conclusion temperature; ΔH, enthalpy change.

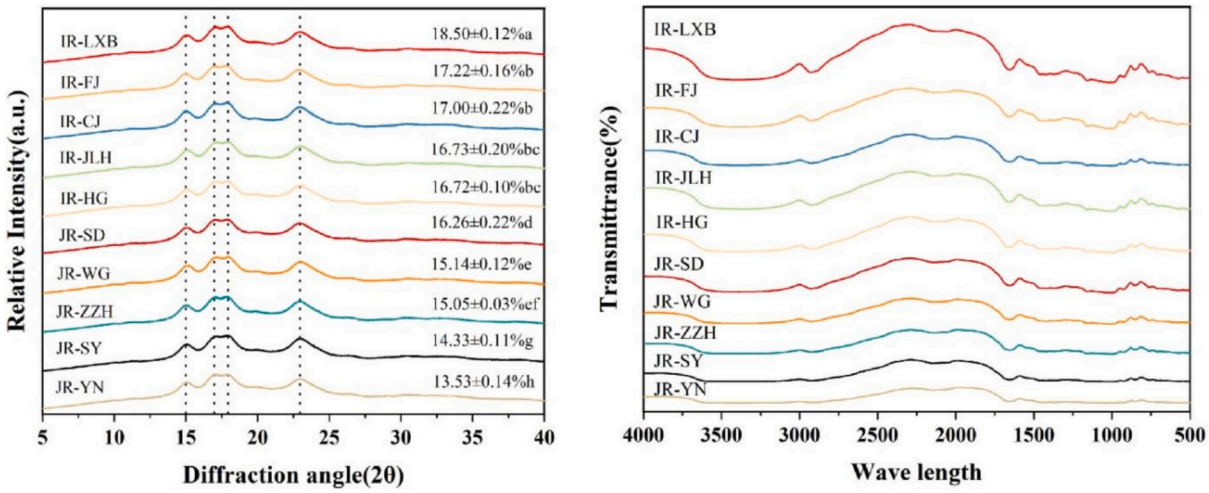

Fig. 2. X-ray diffraction pattern and FTIR spectrogram of different GRF.

proportion of longer chains may form longer crystallites, thereby producing more perfect crystalline structures.

The FTIR spectrum can reflect the short-range order structure present on external region of granule. The bands at 1045 and 1022 cm^{-1} are associated with ordered/crystalline and amorphous regions in starch, respectively. The ratio of absorbance 1045/1022 cm^{-1} is used to quantify the ordered degree (Lin et al., 2019). The absorbance ratios of the ten types of GRF were shown in Table 2, ranging from 0.7155 to 0.6743, with significant differences observed among the GRF ($P < 0.05$). From the perspective of GRF types, the absorbance ratios of IGRF were consistently higher than those of JGRF. Among the different GRF, IR-LXB exhibited the highest absorbance ratio at 1045/1022 cm^{-1} (0.7155), while JR-YN showed the lowest value (0.6743). These results indicate that IGRF, particularly IR-LXB, possesses more short-range ordered structures compared to JGRF, which is consistent with the relative crystallinity results (Table.3). Furthermore, the absorbance ratios of all GRF correspond positively with the proportion of amylopectin branch chains (DP 13–24), as these chains are primarily responsible for the formation of double helix structures (Wang et al., 2017).

3.4. Pasting properties

The gelatinization behavior of starch is a combination of complex processes that occur after gelatinization, including the swelling and rupture of starch granules, the leaching of amylose, and the formation of gels under high energy input (Zhu et al., 2020). Gelatinization capacity determines the thermal processing properties of starch-based foods. The gelatinization parameters of GRF were determined using a Rapid Visco

Analyzer (RVA), and the results are shown in Table 3.

Peak viscosity (PV) reflects the swelling capacity of starch granules and their ability to bind water. The PV of IGRF ranged from 3458.68 cP to 4508.12 cP, while that of JGRF ranged from 2521.75 cP to 3137.42 cP, with significant differences observed among the ten types of glutinous rice flour ($P < 0.05$). Based on the interactions between starch molecules and hydrocolloids during gelatinization, the interaction between amylopectin with long branches and amylose promotes an increase in viscosity. This is because amylopectin with long external chains exhibits behavior similar to amylose during heating, namely leaching from starch granules (Chen et al., 2014). Therefore, the differences in viscosity are closely related to amylose content and the proportion of long branches in amylopectin.

The gelatinization temperature of IGRF ranged from 81.11 °C to 73.83 °C, while that of JGRF ranged from 70.13 °C to 68.81 °C ($P < 0.05$). The gelatinization temperature is positively correlated with amylose content, which is consistent with the results in Table 1; however, the proportion of short branches in amylopectin is negatively correlated with gelatinization temperature. This is because short branches reduce the packing efficiency of starch crystallinity, weaken the stability of the double helix structure, and fail to provide strong interactions to maintain the integrity of swollen granules, resulting in a lower gelatinization temperature (You et al., 2014). This result is also consistent with the gelatinization temperature (PT) data and the branch chain distribution data.

Furthermore, the data showed that the final viscosity (FV) of IGRF (2198.62 cP to 2624.72 cP) was higher than that of JGRF (956.88 cP to 1465.71 cP). FV is attributed to the rearrangement of starch chains in the cooling environment. During cooling, the gel formed after gelatinization restricts the flow of water, ultimately affecting the viscosity of the paste (Sun et al., 2021). Breakdown value (BD) can be used to illustrate the response of starch to shear thinning, with a higher BD value indicating poorer stability of the entire paste system during heating. Within the same glutinous rice variety, BD decreased with decreasing PV, with IR-LXB exhibiting the highest BD value (2392.68 cP) and JR-YN the lowest (1811.57 cP). Setback value (SB) is an indicator of the strength of short-term retrogradation tendency and is positively correlated with amylose content (Yi et al., 2020). From the perspective of glutinous rice types, the SB of IGRF (452.21 cP to 355.46 cP) was higher than that of JGRF (298.56 cP to 229.86 cP), indicating that the gelatinization system of IGRF undergoes a higher degree of short-term retrogradation during the cooling stage. This means that the gel network structure formed by IGRF after gelatinization is more rigid than that of JGRF, resulting in higher hardness and toughness of the entire food system. This difference may further affect the sensory properties of daifuku products, such as elasticity and chewiness.

3.5. Thermal properties

Table 3 summarized the thermodynamic parameters of ten types of GRF from the two categories, including the onset temperature (To), peak temperature (Tp), conclusion temperature (Tc), and enthalpy change (ΔH). Significant differences ($P < 0.05$) were observed in all four parameters between IGRF and JGRF. For IGRF, the To ranged from 76.18 °C to 65.97 °C, the Tp ranged from 80.46 °C to 70.57 °C, the Tc ranged from 84.72 °C to 75.53 °C, and the ΔH ranged from 9.77 J/g to 7.42 J/g. Among these, IR-LXB exhibited the highest values for all four parameters. For JGRF, the To ranged from 62.30 °C to 60.42 °C, the Tp ranged from 68.23 °C to 67.29 °C, the Tc ranged from 75.06 °C to 74.35 °C, and the ΔH ranged from 7.11 J/g to 6.29 J/g. Among these, JR-SD showed the highest values for all four parameters. The order of these parameter values corresponded to the PV. It has been reported that high transition temperatures are caused by high crystallinity, which provides structural stability and makes the granules more resistant to gelatinization. The differences in To and ΔH among different starch varieties may be attributed to variations in the number of long chains in amylopectin. These long chains require higher temperatures to fully dissociate compared to short double helices. These measurement results align with the proportion of long branches in amylopectin (Singh et al., 2006).

3.6. In vitro starch digestibility

Based on the extent and rate of starch digestion, starch can be classified into rapidly digestible starch (RDS), slowly digestible starch (SDS), and resistant starch (RS). From the perspective of the multi-scale structure of starch, the amylose content and the structure of amylopectin significantly influence the structural transformation and digestibility of starch (Chi et al., 2021). Table 4 summarizes the digestibility parameters of the ten types of GRF. The results indicate that, from the perspective of the two types of glutinous rice—indica and japonica—the RDS of japonica glutinous rice is significantly higher than that of indica glutinous rice, while the RS shows the opposite trend. Among them, JR-YN has the highest RDS (76.38 %) and the lowest RS (18.20 %) among the ten types of GRF. For the other four JGRF samples, the RDS gradually decreases as viscosity increases, while the RS gradually increases. In indica glutinous rice, the trends of RDS and RS are consistent with those of japonica glutinous rice: as viscosity increases, RDS decreases and RS increases. Specifically, IR-LXB has the lowest RDS (53.97 %) and the highest RS (38.69 %) among all the GRF, while IR-FJ, IR-CJ, and IR-JLH show no significant differences in RDS and RS values. The variation in RDS among the ten types of glutinous rice is negatively correlated with amylose content and positively correlated with RS content. This is because a higher amylose content can delay starch swelling and disruption during processing, thereby maintaining a semi-crystalline structure during conventional cooking, which inhibits enzyme-starch interactions and reduces digestibility (Chung et al., 2011). During cooling and digestion, leached amylose recombines to form a gel network containing stable double helices and strong microcrystals (Zheng et al., 2023). Additionally, numerous studies have shown that the chain length of amylopectin in starch influences its digestibility. Amylopectin chains with degrees of polymerization (DP) of 13–24 and 25–36 tend to form double helices or microcrystals during cooling and retrogradation, promoting the formation of rigid crystalline structures, which significantly inhibit enzymatic digestion (Sasaki et al., 2009). Specifically, the RDS value is negatively correlated with the proportion of these chain lengths, indicating that the proportion of amylopectin chains with DP > 13 in GRF affects its digestibility, resulting in lower digestibility for such flours. This aligns with the proportion of chain lengths described in the previous section (Table 2). Therefore, the digestibility of GRF with different PV, which may lead to differences in the quality of the final products.

3.7. Rheological properties

Rheological properties describe the deformation and fluidity of a material under the influence of mixing, transport, and external forces. Fig. 4 (AB, DE) illustrated the graphs of G' and G" versus frequency for two distinct types of GRF. The observation that G' was consistently higher than G" throughout the frequency scan, with no crossover between these two moduli point, and indicated that these ten types of GRF gel systems were shown typical weak gels, as reported in reference (Yousefi & Razavi, 2015). The tan δ values of GRF with different viscosity in the two types were found to be much less than 1, and the GRF batters were solid-like. The tan δ values exhibited a decreasing and then increasing trend as the PV of the two types of GRF increased from 3458.68 to 4508.12 cP for IGRF and from 2521.75 to 3137.42 cP for JGRF, respectively. Fig. 2 C and F illustrated the inverse relationship between tan δ values at 10 Hz and the PV of GRF. Higher tan δ values indicated that the GRF paste has more free water and exhibited less solid-like behavior due to the poorer water-holding capacity of the starch granules, which made it more difficult for water to penetrate.

Table 4
Digestibility parameters obtained from the in vitro digestibility kinetics of different GRF samples.

	IGRF					JGRF				
	IR-LXB	IR-FJ	IR-CJ	IR-JLH	IR-HG	JR-SD	JR-WG	JR-ZZH	JR-SY	JR-YN
RDS (%)	53.97 ± 0.23^{h}	58.26 ± 0.17^{g}	58.35 ± 0.36^{g}	58.61 ± 0.11^{g}	64.70 ± 1.34^{f}	69.29 ± 1.20^{e}	73.35 ± 0.64^{d}	73.40 ± 0.57^{c}	75.63 ± 0.32^{b}	76.38 ± 0.25^{a}
SDS (%)	7.340 ± 0.07^{a}	6.463 ± 0.20^{bc}	6.371 ± 0.12^{bc}	6.092 ± 0.32^{c}	5.424 ± 0.41^{d}	4.997 ± 0.21^{de}	1.802 ± 0.71^{h}	4.490 ± 0.45^{fg}	4.421 ± 0.25^{fg}	2.151 ± 0.43^{h}
RS (%)	38.69 ± 0.17^{a}	38.02 ± 0.27^{a}	35.28 ± 0.34^{b}	35.30 ± 0.31^{b}	33.15 ± 0.25^{c}	25.72 ± 0.22^{d}	24.85 ± 0.11^{d}	22.11 ± 0.08^{e}	19.95 ± 0.15^{f}	18.20 ± 0.18^{g}
SDS + RS (%)	46.03 ± 1.01^{a}	44.49 ± 0.30^{b}	41.65 ± 0.67^{c}	41.39 ± 0.53^{d}	38.57 ± 0.31^{e}	30.72 ± 0.26^{f}	26.65 ± 0.15^{g}	26.60 ± 0.14^{h}	24.37 ± 0.13^{i}	20.35 ± 0.20^{j}

Means values ± standard deviation, n = 3. Different superscript letters in the same row in69.296.092dicate significant differences at $P < 0.05$.

However, when starch granules were spontaneously hydrated in water the starch granules absorbed water and swelled, leaching amylose and amylopectin. This process also led to a less elastic and more viscous paste. GRF batters typically have a more elastic gel-like network structure due to the stronger gel network strength, which is reflected in lower tan δ values. In this study, the pastes of IR-LXB, IR-FJ, IR-CJ, and JR-SD exhibited lower tan δ values and a more stable and ordered structure. This may contribute to the production of Daifuku with consistent quality.

3.8. Microstructure and morphology

All ten types of GRF successfully produced Daifuku with acceptable appearance, and Daifuku made from the same type of GRF exhibited a certain degree of similarity in their top-view appearance (Fig. 4 A_1&A_2). The length, width, height, and whiteness data of the Daifuku were detailed in Table 5. With a gradient difference in PV, the side-view appearance of the Daifuku showed significant variations (Fig. 5 B_1&B_2). It was clearly observed that as PV decreased, the height of the Daifuku gradually reduced. Daifuku made from JGRF generally had greater length and width compared to those made from IGRF, while Daifuku made from IGRF exhibited greater height overall than those made from JGRF. This indicated that Daifuku made from IGRF were taller and more three-dimensional, whereas those made from JGRF showed varying degrees of flattening. Among them, Daifuku made from IR-LXB had the maximum height of 3.36 cm after freezing, followed by those made from IR-FJ and JR-SD at 3.02 cm, and JR-WG at 2.92 cm. Notably, Daifuku made from IR-LXB had some gaps between the outer skin and the inner cream, while those made from IR-FJ, JR-SD, and JR-WG showed tight contact between the skin and cream, which helped maintain a round and plump appearance. Despite the incomplete adhesion between the skin and cream in IR-LXB Daifuku, its high viscosity characteristics still allowed it to retain good three-dimensionality. In contrast, Daifuku made from IR-HG, JR-YN, and JR-SY showed significant height reduction, with JR-YN having the lowest height at 2.49 cm, a 25.90 % decrease compared to the tallest IR-LXB Daifuku. Additionally, in the side-view images of daifuku made from JLH and HG in IGRF, as well as ZZH, SY, and YN in JGRF, noticeable bubbles were observed, mostly distributed on the inner surface near the edges. The low viscosity of these flours resulted in poor adhesion between the skin and filling, further compromising the structural integrity of the Daifuku. These results demonstrated that Daifuku made from IGRF were better able to maintain their height, while those made from JGRF were more prone to collapsing. In terms of whiteness, except for IR-HG, which had a whiteness value exceeding 90, the other samples ranged between 88 and 89, showing little difference.

Furthermore, the scanning electron microscopy (SEM) images in Fig. 3C1&C2 allowed for a closer examination of the internal gel network structure of the Daifuku skin. The results revealed that Daifuku made from IR-LXB, IR-FJ, JR-SD, and JR-WG had dense and uniform internal structures with only minor cracks and no visible pores. Daifuku made from IR-CJ exhibited a relatively complete gel network structure but with more pronounced cracks compared to the former four. In contrast, the microstructural images of daifuku made from IR-JLH, IR-HG, JR-ZZH, JR-SY, and JR-YN showed noticeable bubble-like pores and deep cracks, with IR-HG and JR-YN having the highest number and largest size of pores. This indicates that the gel systems formed by these flours after gelatinization were relatively loose and less cohesive.

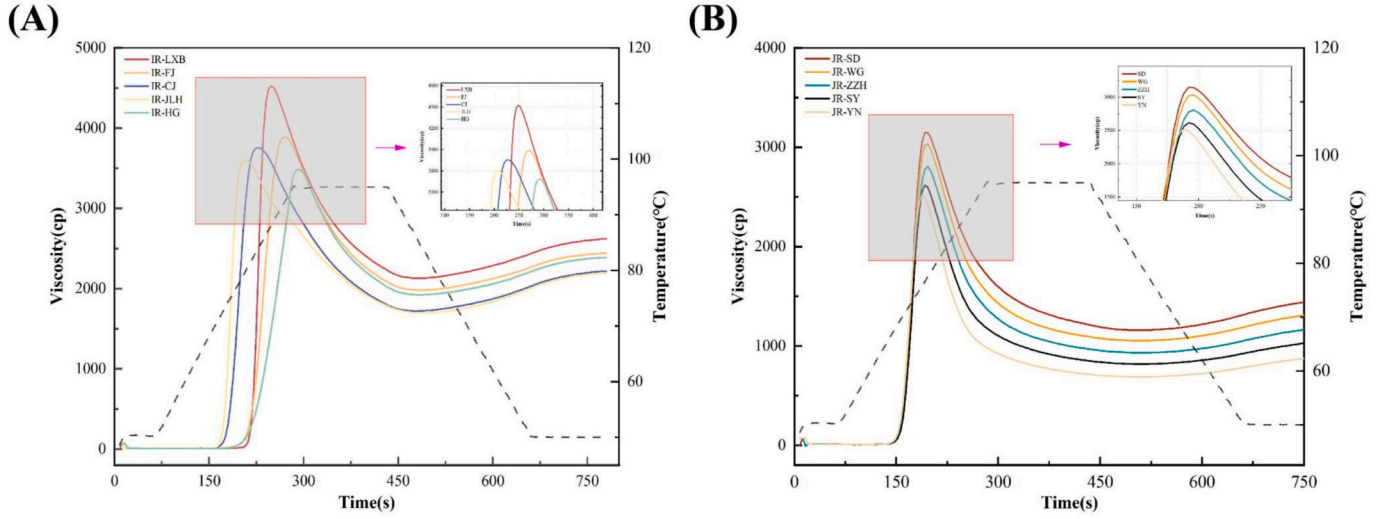

Fig. 3. Pasting viscosity profiles of five IGRF (A) and JGRF (B).

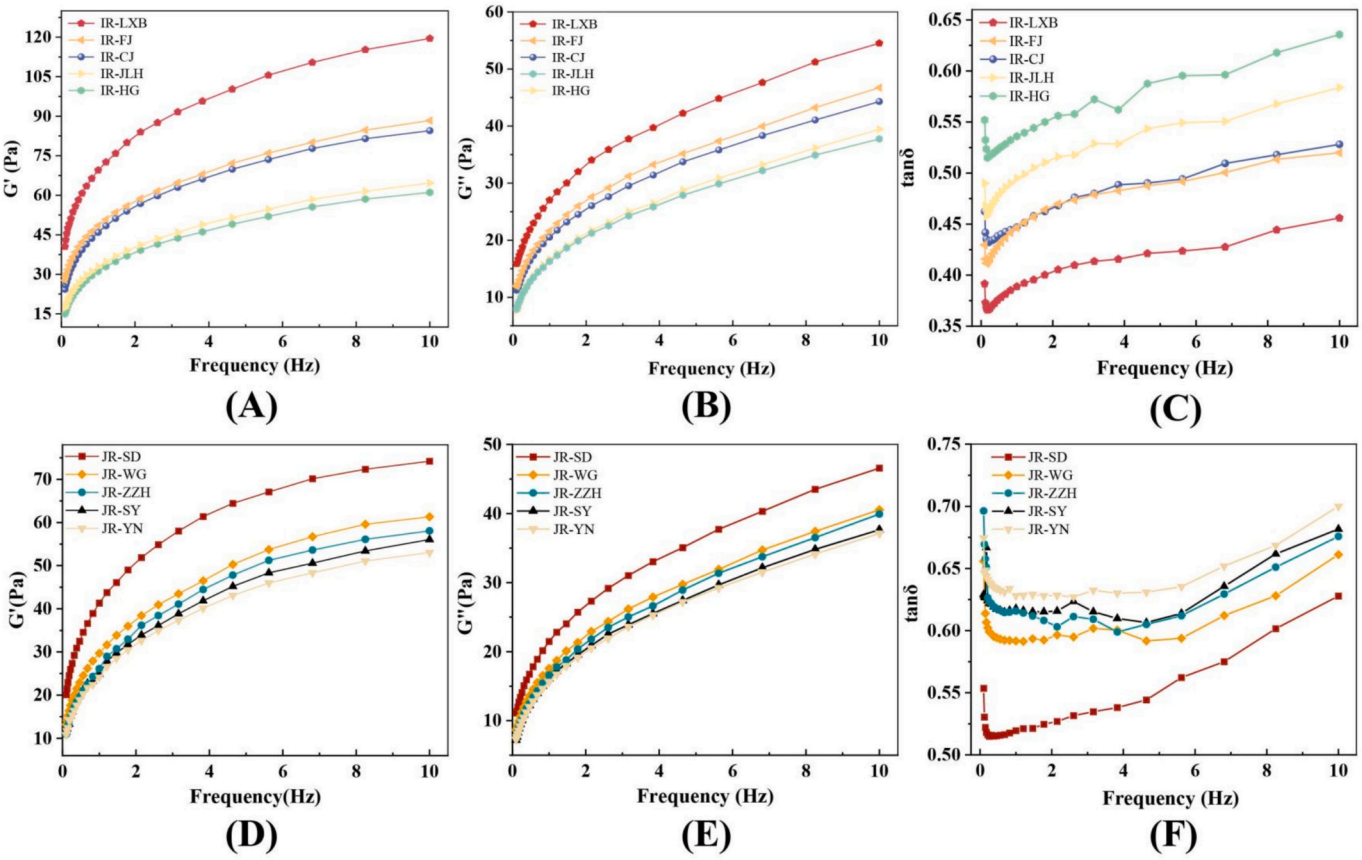

Fig. 4. Rheological properties of GRF. The elastic modulus (G') (A) (D), viscous modulus (G") (B) (E) and loss tangent (tan δ) (C) (F).

Table 5
Apparent characteristics of Daifuku prepared from different GRF.

	IGRF					JGRF				
	IR-LXB	IR-FJ	IR-CJ	IR-JLH	IR-HG	JR-SD	JR-WG	JR-ZZH	JR-SY	JR-YN
Length (cm)	5.60 ± 0.07^{bcd}	5.55 ± 0.07^{bcd}	5.45 ± 0.14^{d}	5.50 ± 0.14^{cd}	5.55 ± 0.07^{bcd}	5.65 ± 0.01^{abc}	5.68 ± 0.01^{a}	5.78 ± 0.01^{a}	5.78 ± 0.02^{ab}	5.79 ± 0.02^{a}
Width (cm)	5.50 ± 0.05^{d}	5.45 ± 0.08^{d}	5.55 ± 0.04^{cd}	5.45 ± 0.04^{d}	5.55 ± 0.01^{cd}	5.64 ± 0.01^{bc}	5.66 ± 0.01^{bc}	5.78 ± 0.01^{a}	5.73 ± 0.04^{ab}	5.79 ± 0.01^{a}
Length / Width	1.02 ± 0.00^{a}	1.01 ± 0.03^{a}	0.98 ± 0.01^{b}	1.00 ± 0.01^{ab}	1.00 ± 0.01^{ab}	1.00 ± 0.00^{ab}	1.00 ± 0.00^{ab}	1.00 ± 0.00^{ab}	1.00 ± 0.01^{ab}	1.00 ± 0.00^{ab}
Height (cm)	3.36 ± 0.02^{a}	3.02 ± 0.03^{bc}	2.84 ± 0.00^{e}	2.91 ± 0.02^{d}	2.81 ± 0.01^{ef}	3.02 ± 0.00^{bc}	2.98 ± 0.02^{d}	2.74 ± 0.00^{g}	2.78 ± 0.00f^{g}	2.49 ± 0.00^{h}
The whiteness of Daifuku	89.89 ± 0.05^{c}	88.84 ± 0.18^{f}	89.82 ± 0.05^{c}	90.35 ± 0.04^{b}	91.70 ± 0.16^{a}	89.51 ± 0.06^{d}	89.26 ± 0.04^{e}	88.27 ± 0.05^{h}	88.52 ± 0.03^{g}	88.46 ± 0.06^{gh}

Means values ± standard deviation, n = 3. Different superscript letters in the same row indicate significant differences at $P < 0.05$.

3.9. Textural properties

The results of the effect of viscosity on the textural properties of Daifuku were presented in Table 6. In IGRF, the variation of hardness values with viscosity decreased significantly, from 312.15 g to 220.91 g. In JGRF, the variation of hardness values with viscosity followed a similar trend and was generally lower than that of IGRF. This decrease was observed to be from 298.99 g to 165.11 g. The hardness is primarily influenced by the retrogradation of amylose and amylopectin (Du et al., 2022). Daifuku with high PV exhibited a higher proportion of medium and long branched chains (B_2 and B_3) (Table 2 and Table 3), indicating a higher retrogradation rate (higher hardness) of the gel system formed by the paste. This was, especially evident in IR-LXB, which had the highest proportion of B_2 and B_3 chains and thus the highest hardness, resulting in an improved retrogradation rate. Adhesiveness is the negative force region between the first and second bites, corresponding to the tan δ value, which directly reflects the adhesiveness properties of GRF (Wang et al., 2019). The higher value of adhesiveness means that the food is more adhesive to teeth after mastication (Li et al., 2018). Among the samples, IR-FJ and IR-JLH exhibited relatively higher values of 123.20 g•s and 121.08 g•s, respectively, indicating that the Daifuku prepared from this GRF was difficult to chew and swallow. There was minimal variation in the adhesiveness of Daifuku prepared from IR-LXB, IR-CJ, and IR-HG. JR-SD and JR-ZZH exhibited the highest adhesiveness of the JGRF, while JR-YN exhibited the lowest. In addition, resilience and springiness indicate the ability of Daifuku dough to return to its original shape and the ability to return to its original height after the first compression, respectively. There was minimal difference in resilience between the two types of GRF. However, when comparing the dough springiness of IGRF and JGRF, it can be observed that the former

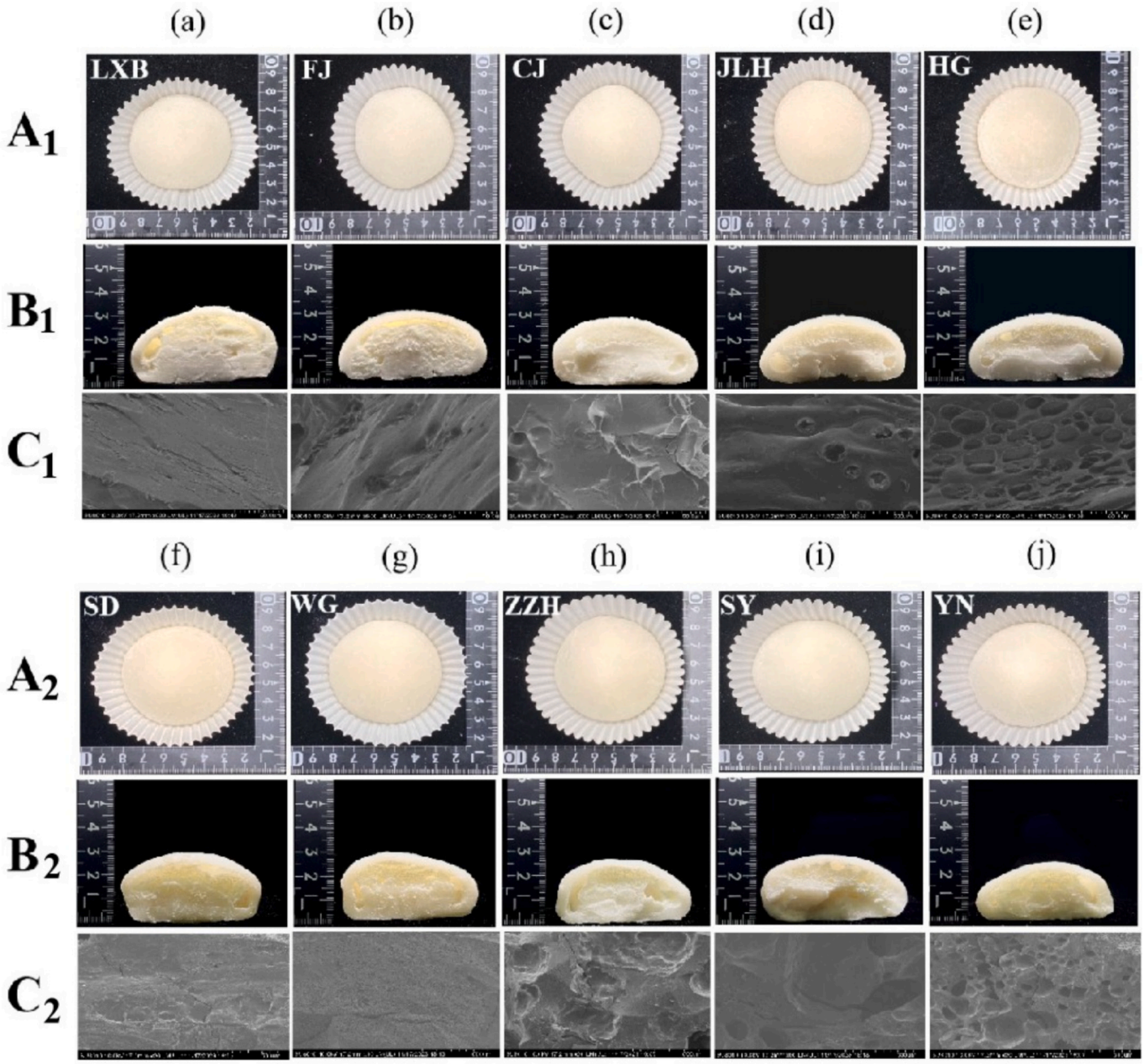

Fig. 5. Appearance, section, and microstructure of Daifuku prepared from different GRF.

exhibited superior elasticity compared to the latter. This can be attributed to the higher viscosity of IGRF, which resulted in a stronger dough with a higher Springiness. In general, IGRF demonstrated superior performance in the comprehensive assessment of the product's textural characteristics.

3.10. Lf-NMR

Moisture distribution in frozen Daifuku is crucial for maintaining the appearance and skin texture after transportation. As shown in Fig. 6, transverse relaxation time (T_2) was measured after 24 h, −18 °C freezing and 30 min thawing to investigate the moisture mobility of Daifuku. Three peaks T_{21}, T_{22} and T_{23} were observed in Fig. 6A, which represent tightly bound water, weakly bound water and free water, respectively. In the relaxation time profile (T_2), the larger the T_2, the weaker the water molecules in this state were bound by the gel network structure and the greater the water mobility. Conversely, the smaller the T_2, the stronger the water molecules in this state were bound by the gel network structure and the weaker the water mobility (Chen et al., 2017). There were obvious differences in the appearance of Daifuku prepared from different GRF after freezing, which may be due to the differences in the binding capacity of starch gel networks for water molecules. In particular, after freezing, the water molecules inside the starch gel network formed ice crystals, and after thawing, the gel system with poor binding capacity had stronger water mobility (Jia et al., 2019), which would further cause the collapse of the body shape, as the decrease of PV value, the peaks of T_{21} unchanged, while the T_{23} increased. According to the LF-NMR theory, the higher T_2 means weaker water mobility and weaker interaction between the water and samples (Chen et al., 2017). The weak ability of the gel structure to bind water promotes the formation of large ice crystals after freezing, and after thawing, the water from melted ice crystals does not return to its original state and cannot be reabsorbed, resulting in the flattening of the body shape of Daifuku and dry, hard appearance. As shown by IR-HG and JR-YN in Fig. 5. The

Table 6
Textural properties of Daifuku made from different types of GRF.

	IGRF					JGRF				
	IR-LXB	IR-FJ	IR-CJ	IR-JLH	IR-HG	JR-SD	JR-WG	JR-ZZH	JR-SY	JR-YN
Hardness (g)	312.15 ± 2.40^{a}	303.81 ± 6.02^{abc}	278.24 ± 11.97^{abc}	271.67 ± 12.30^{c}	220.91 ± 21.03^{d}	298.99 ± 8.91^{ab}	276.83 ± 13.48^{bc}	219.64 ± 13.78^{d}	219.65 ± 13.58^{d}	165.11 ± 22.09^{e}
Adhesiveness (g● s)	114.23 ± 12.10^{de}	123.20 ± 14.83^{e}	113.04 ± 15.67^{cde}	121.08 ± 6.02^{de}	115.34 ± 4.23^{de}	104.79 ± 34.70^{bcd}	75.00 ± 8.95^{bc}	101.87 ± 17.07^{bcd}	83.56 ± 4.79^{abc}	62.54 ± 2.32^{a}
Resilience (%)	24.66 ± 1.60^{a}	24.37 ± 1.36^{a}	24.37 ± 0.33^{a}	25.89 ± 1.36^{b}	24.75 ± 0.32^{a}	20.53 ± 0.35^{cd}	21.81 ± 0.11^{c}	21.03 ± 0.60^{cd}	21.29 ± 0.84^{c}	19.03 ± 1.47^{d}
Cohesiveness	0.59 ± 0.01^{bc}	0.61 ± 0.01^{a}	0.61 ± 0.01^{a}	0.59 ± 0.01^{bc}	0.58 ± 0.01^{c}	0.61 ± 0.00^{a}	0.61 ± 0.00^{a}	0.60 ± 0.02^{ab}	0.55 ± 0.01^{d}	0.53 ± 0.00^{d}
Springiness (%)	95.31 ± 0.90^{ab}	95.24 ± 1.33^{ab}	95.04 ± 1.02^{ab}	94.41 ± 0.47^{ab}	94.13 ± 1.45^{ab}	96.22 ± 1.33^{a}	96.14 ± 0.42^{a}	95.40 ± 0.29^{ab}	94.49 ± 0.04^{ab}	94.05 ± 7.05^{b}
Gumminess	205.31 ± 9.44^{b}	253.27 ± 8.86^{a}	190.50 ± 2.53^{b}	202.80 ± 17.78^{b}	214.86 ± 17.90^{b}	206.06 ± 20.98^{b}	175.47 ± 28.72^{b}	117.18 ± 7.84^{c}	120.36 ± 7.36^{c}	99.11 ± 15.98^{c}
Chewiness (g)	201.95 ± 2.47^{a}	193.87 ± 9.88^{ab}	184.33 ± 11.55^{abc}	181.06 ± 2.53^{abc}	172.06 ± 11.52^{bc}	189.86 ± 11.75^{abc}	180.84 ± 23.64^{abc}	165.41 ± 20.89^{c}	119.33 ± 11.94^{d}	113.46 ± 6.98^{d}

Means values ± standard deviation, n = 3. Different superscript letters in the same row indicate significant differences at $P < 0.05$.

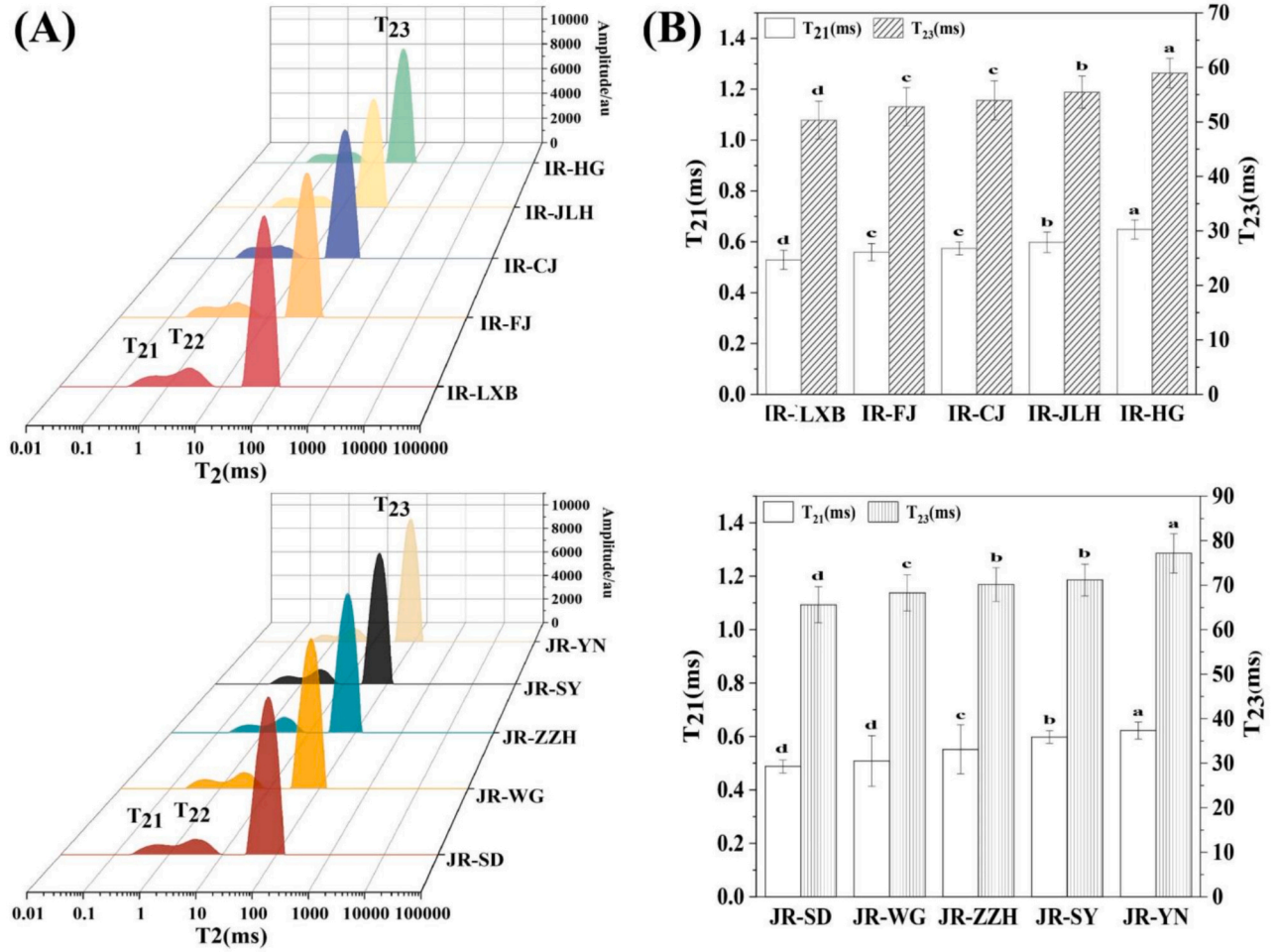

Fig. 6. T_2 inversion map of Daifuku made from different GRF. A typical T_2 relaxation time distribution curve (A), T_{21} and T_{23} of Daifuku (B).

improved shape retention observed in Daifuku may be attributed to the high proportion of long-branched amylopectin structures presented within the interior of the product. These structures were capable of folding to create a more intricate spatial configuration during retrogradation, which in turn leaded to the formation of a more robust gel network structure. Consequently, the binding capacity for water molecules was enhanced, resulting in a softer epidermis. Therefore, the ratio of long-branched chains in GRF played a pivotal role in determining the final product's shape characteristics.

3.11. Sensory evaluation

Sensory evaluation serves as a critical criterion and decisive factor for optimizing food processing and enhancing product quality. For Daifuku, the most favored sensory characteristics among consumers include a complete, plump, and smooth appearance, the absence of off-

flavors, a distinct aroma of glutinous rice, and a soft, non-sticky texture. Fig. 7A&B present radar charts of sensory evaluations for mochi prepared from two types of GRF. As shown in the figures, mochi made from IR-LXB flour exhibited the highest overall acceptability, receiving the highest scores for appearance and chewiness. Mochi prepared from IR-FJ and IR-CJ flours scored closely to IR-LXB, with superior performance in elasticity and mouthfeel, respectively. In contrast, mochi made from IR-JLH and IR-HG flours received lower overall scores, consistent with the morphological observations (Fig. 5). Notably, however, mochi prepared from IR-HG flour achieved the highest score for color, displaying a bright, white, and glossy appearance that was more appealing to consumers. This is primarily attributed to the lower protein content in IR-HG, which effectively reduced yellowing and darkening during the cooking process (Phongthai et al., 2017).

Among the JGRF-type GRF, all five samples had higher protein content than the IGRF-type but exhibited lower viscosity. Consequently, except for the aroma index, the average scores for the other six sensory indicators of mochi prepared from JGRF flours were lower than those of IGRF. The higher protein content enhanced the distinctive flavor of glutinous rice. Volunteers reported that mochi made from JGRF, particularly JR-SY and JR-YN, had a noticeably sticky and dense texture, being moister and more adhesive than those made from IGRF, which made swallowing difficult and left a lingering sensation in the mouth. Additionally, studies suggest that certain proteins may restrict starch swelling during gelatinization, leading to reduced viscosity (Li et al., 2018).

3.12. Principal component analysis (PCA) and correlation analysis

The relationship between different GRF and the quality of Daifuku was summarized in Fig. 8A. PCA combined with cluster analysis can simplify the comprehensive evaluation indices. Principal Component 1 (PC1) and Principal Component 2 (PC2) account for 74.7 % of the total variance. Therefore, PC1-PC2 reflected the major contributions to the response variables. The distance and position on the biplot can reflect the quality of Daifuku. In Fig. 8A, GRF with different PV was divided into three groups based on the corresponding quality of Daifuku. The first group was located in the first quadrant and included JR-SD, JR-WG, and IR-LXB. These Daifuku had a smooth appearance with a certain hardness and chewiness while maintaining a good three-dimensional shape. The food system had a compact and resilient structure for an enjoyable eating experience. The second group consisted of JR-ZZH, JR-SY, JR-YN, which were located in the second and third quadrants, these Daifuku had a greater width and length, indicating a flatter shape. The third group was located in the fourth quadrant and consisted of IR-CJ, IR-FJ, IR-HG, and IR-JLH, which have high cohesiveness and viscosity. These Daifuku were able to maintain a certain body shape, but the overall sensory experience was lower than the first group. This suggested that the maintenance of the appearance and shape of Daifuku was closely related to the texture of the gel network within the system, and that too low viscosity may lead to a loosely structured food system, poor shape retention, and a decreased sensory experience.

Furthermore, the correlations between the sensory evaluation indexes of Daifuku and the properties and structural characteristics of GRF were constructed using correlation analysis (Fig. 8B). Among these, PV, ΔH, and SB value in gelatinization property, as well as temperature variation in thermal property demonstrated significant positive correlations with the textural characteristics of hardness, cohesiveness, resilience, chewiness, gumminess, springiness, and height of Daifuku. In addition, the content of free-flowing water in the moisture distribution exhibited a significant positive correlation with the length and width of Daifuku. This may be attributed to the fact that T_{23} represents free-flowing water, and the weaker morphology of Daifuku's own gel system with a weak moisture retention capacity was more prone to flattening. The percentage of amylopectin DP $>$ 37 was significantly positively related to the height of Daifuku. Long-branched chains were able to form double helices more effectively in the gel system. This resulted in a more compact gel structure with enhanced morphology retention and water retention abilities. Therefore, the hypothesized mechanisms of action of the two types of GRF were shown in Fig. 9. A higher proportion of amylose could make a moderate short-term regeneration of the gel, which can retain Daifuku morphological in the early stage of storage without collapse. The higher proportion of medium and long-branched chains (B_2 and B_3) in IGRF contributes to the formation of more double-helical structures during the retrogradation process of the paste, which in turn facilitated the folding of the paste into a gel network with a stronger structure and greater water retention capacity. The effects of dehydration and shrinkage were minimized, resulting in a softer and smoother product texture (Tao et al., 2019).

4. Conclusion

This study selected five types of glutinous rice from both indica and japonica varieties with different PV as the starting point. GRF was prepared using a semi-dry method, and the differences in the branch chain structure of amylopectin among the ten types of GRF were analyzed. From the perspectives of basic composition, crystalline structure, gelatinization properties, thermal properties, digestibility kinetics, and

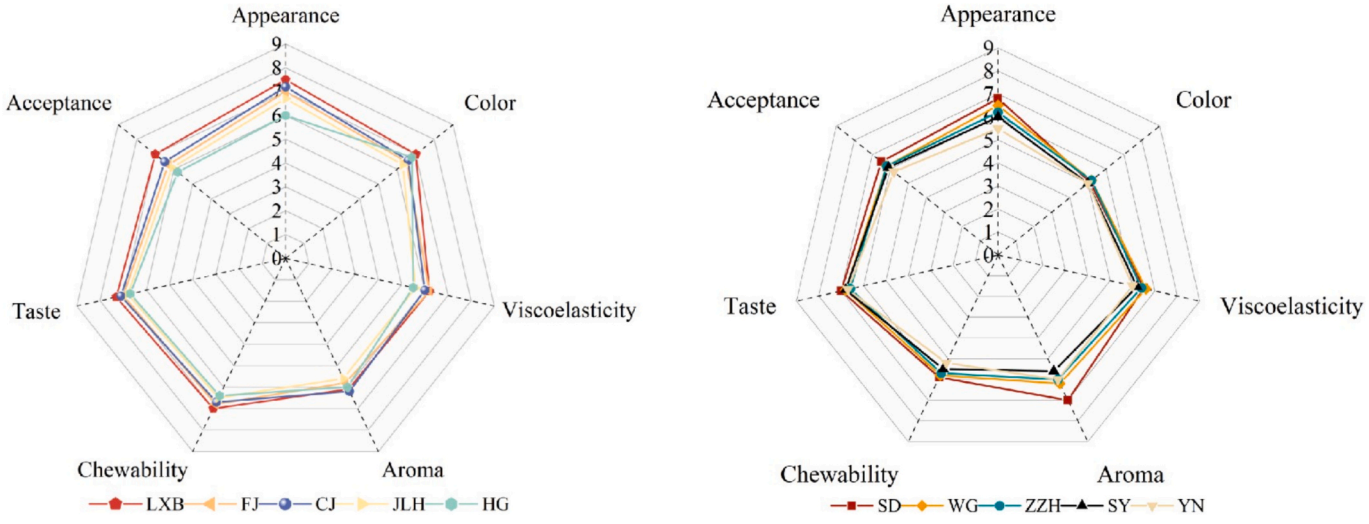

Fig. 7. Radar chart for sensory evaluation of Daifuku prepared from IGRF (A) and JGRF (B).

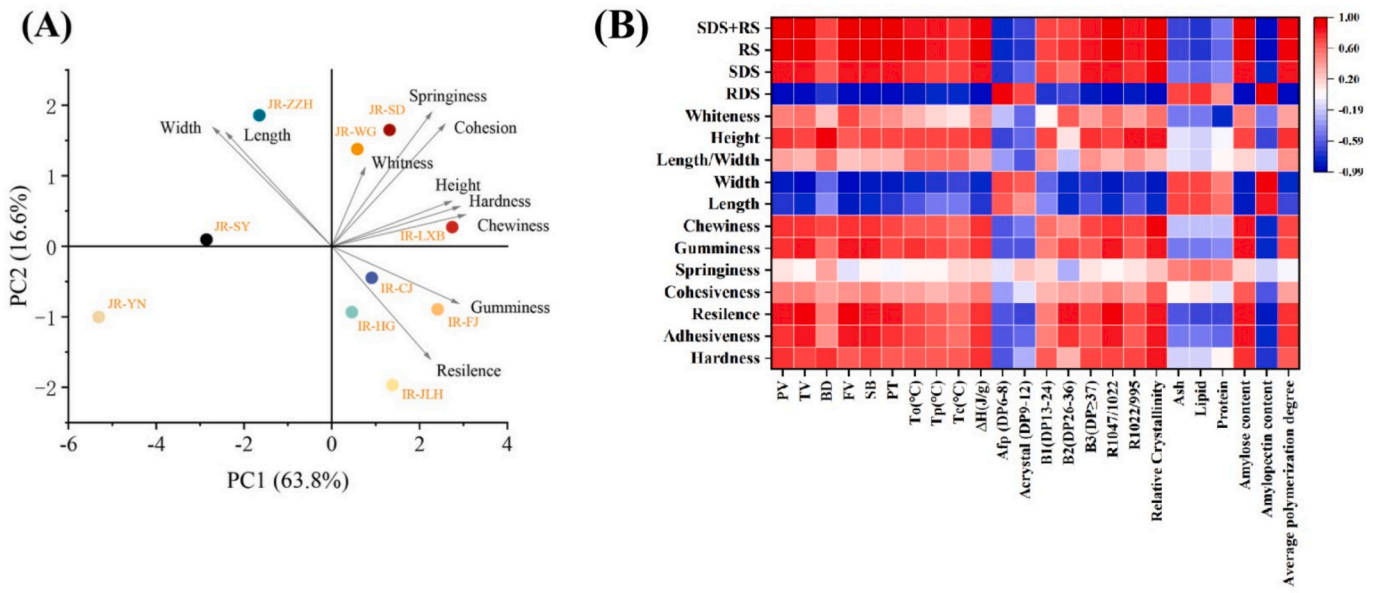

Fig. 8. Principal component analysis (A) and correlation heat map (B) of IGRF Daifuku and JGRF Daifuku.

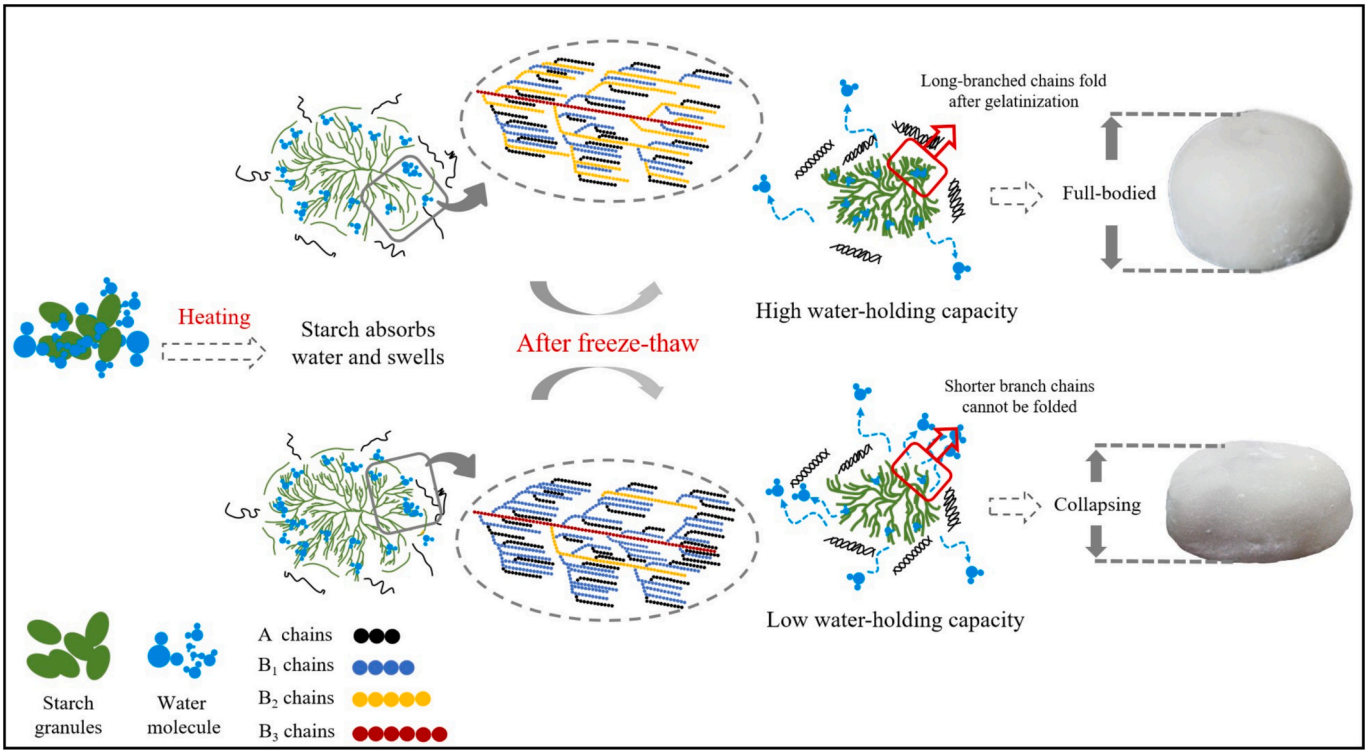

Fig. 9. A schematic diagram describing the potential mechanism of action of changes in the appearance of Daifuku prepared from different GRF after freezing.

rheological properties, the influence of amylopectin branch chain structure on viscosity and flour quality differences was elucidated. The study found that the gelatinization temperature, relative crystallinity, 1047/1022 ratio, average chain length of amylopectin, proportion of long branches, and SDS and RS content of IGRF were significantly higher than those of JGRF, while the proportion of short branches in amylopectin was lower than that of JGRF. At the same time, Daifuku was prepared from different GRF, and the differences in morphological characteristics were recorded. The moisture distribution on the surface was measured, and sensory evaluations were conducted. The flour characteristics were correlated with the final product quality. The results showed that Daifuku prepared from IGRF had a brighter and fuller color compared to those prepared from JGRF, with IR-LXB producing the best morphological characteristics. Additionally, Daifuku made from IGRF performed better in terms of acceptability, appearance, chewiness, and taste. Overall, IGRF has a higher proportion of medium and long branches in amylopectin, which can form more stable double helix structures, exhibit higher relative crystallinity and short-range molecular order, and have lower digestibility. Therefore, IGRF can form a more rigid and dense gel network structure after gelatinization, resulting in more stable Daifuku quality. This study provides scientific guidance for selecting GRF suitable for Daifuku production and

establishes a theoretical foundation for producing Daifuku with uniform and stable quality.

CRediT authorship contribution statement

Yu Tian: Writing – original draft, Methodology, Investigation, Data curation. **Jiaxin Li:** Writing – review & editing, Data curation. **Mengzi Nie:** Investigation. **Lili Wang:** Validation. **Liya Liu:** Supervision. **Fengzhong Wang:** Methodology, Conceptualization. **Li-Tao Tong:** Project administration, Funding acquisition, Conceptualization.

Declaration of competing interest

The authors declare that they have no known competing financial interests or personal relationships that could have appeared to influence the work reported in this paper.

Acknowledgements

The work was kindly funded by National Key Research and Development Program of China (2024YFE0111500) and the Key tasks of Zhongyuan Research Center, Chinese Academy of Agricultural Sciences (ZYZX2023010108).

Appendix A. Supplementary data

Supplementary data to this article can be found online at https://doi.org/10.1016/j.fochx.2025.102423.

Data availability

Data will be made available on request.

References

Boulemkahel, S., Betoret, E., Benatallah, L., & Rosell, C. M. (2021). Effect of low pressures homogenization on the physico-chemical and functional properties of rice flour. *Food Hydrocolloids, 112*, Article 106373. https://doi.org/10.1016/j.foodhyd.2020.106373

Chen, L., Tian, Y., Tong, Q., Zhang, Z., & Jin, Z. (2017). Effect of pullulan on the water distribution, microstructure and textural properties of rice starch gels during cold storage. *Food Chemistry, 214*, 702–709. https://doi.org/10.1016/j.foodchem.2016.07.122

Chen, L., Tong, Q., Ren, F., & Zhu, G. (2014). Pasting and rheological properties of rice starch as affected by pullulan. *International Journal of Biological Macromolecules, 66*, 325–331. https://doi.org/10.1016/j.ijbiomac.2014.02.052

Chi, C., Li, X., Huang, S., Chen, L., Zhang, Y., Li, L., & Miao, S. (2021). Basic principles in starch multi-scale structuration to mitigate digestibility: A review. *Trends in Food Science & Technology, 109*, 154–168. https://doi.org/10.1016/j.tifs.2021.01.024

Chi, C., Li, X., Zhang, Y., Chen, L., & Li, L. (2018). Understanding the mechanism of starch digestion mitigation by rice protein and its enzymatic hydrolysates. *Food Hydrocolloids, 84*, 473–480. https://doi.org/10.1016/j.foodhyd.2018.06.040

Chochkov, R., Savova-Stoyanova, D., Papageorgiou, M., Rocha, J. M., Gotcheva, V., & Angelov, A. (2022). Effects of teff-based sourdoughs on dough rheology and gluten-free bread quality. *Foods, 11*(7), 1012. https://doi.org/10.3390/foods11071012

Chuang, G. C. C., & Yeh, A. I. (2006). Rheological characteristics and texture attributes of glutinous rice cakes (mochi). *Journal of Food Engineering, 74*(3), 314–323. https://doi.org/10.1016/j.jfoodeng.2005.03.001

Chung, H. J., Liu, Q., Lee, L., & Wei, D. (2011). Relationship between the structure, physicochemical properties and in vitro digestibility of rice starches with different amylose contents. *Food Hydrocolloids, 25*(5), 968–975. https://doi.org/10.1016/j.foodhyd.2010.09.011

Du, Y., Zhang, M., Mujumdar, A. S., Phuhongsung, P., & Yang, C. (2022). Effect of addition of rice flour and yeast on improving 3D printing of fermented dough. *Journal of Food Processing and Preservation, 46*(11), Article e17016. https://doi.org/10.1111/jfpp.17016

Gayin, J., Abdel-Aal, E. S. M., Manful, J., & Bertoft, E. (2016). Unit and internal chain profile of African rice (Oryza glaberrima) amylopectin. *Carbohydrate Polymers, 137*, 466–472. https://doi.org/10.1016/j.carbpol.2015.11.008

Geng, D. H., Zhou, S., Wang, L., Zhou, X., Liu, L., Lin, Z., & Tong, L. T. (2020). Effects of slight milling combined with cellulase enzymatic treatment on the textural and nutritional properties of brown rice noodles. *Lwt, 128*, Article 109520. https://doi.org/10.1016/j.lwt.2020.109520

Gong, X., Li, J., Liu, Z., Xu, X., Wang, A., Nie, M., & Tong, L. T. (2023). New insights into influence of green composite modification on the structure, digestive, and physicochemical properties of rice flour. *LWT, 189*, Article 115491. https://doi.org/10.1016/j.lwt.2023.115491

He, Y., Guo, J., Ren, G., Cui, G., Han, S., & Liu, J. (2020). Effects of konjac glucomannan on the water distribution of frozen dough and corresponding steamed bread quality. *Food Chemistry, 330*, Article 127243. https://doi.org/10.1016/j.foodchem.2020.127243

He, Y., Wang, A., Chen, Z., Nie, M., Xi, H., Gong, X., … Tong, L. T. (2023). Effects of egg powder on the structure of highland barley dough and the quality of highland barley bread. *International Journal of Biological Macromolecules, 240*, Article 124376. https://doi.org/10.1016/j.ijbiomac.2023.124376

Honda, Y., Saito, Y., Katsumi, N., Nishikawa, M., & Takagi, H. (2023). Physicochemical properties of starch in rice flour with different hardening rates of glutinous rice cake (mochi). *Journal of Cereal Science, 112*, Article 103687. https://doi.org/10.1016/j.jcs.2023.103687

Huang, J., Wang, Z., Fan, L., & Ma, S. (2022). A review of wheat starch analyses: Methods, techniques, structure and function. *International Journal of Biological Macromolecules, 203*, 130–142. https://doi.org/10.1016/j.ijbiomac.2022.01.149

Jia, R., Jiang, Q., Kanda, M., Tokiwa, J., Nakazawa, N., Osako, K., & Okazaki, E. (2019). Effects of heating processes on changes in ice crystal formation, water holding capacity, and physical properties of surimi gels during frozen storage. *Food Hydrocolloids, 90*, 254–265. https://doi.org/10.1016/j.foodhyd.2018.12.029

Jiang, H., McClements, D. J., Dai, L., Qin, Y., Ji, N., Xiong, L., … Sun, Q. (2024). Effects of moisture content and retrogradation on structure and properties of indica rice flour and starch gels. *Food Hydrocolloids, 150*, Article 109657. https://doi.org/10.1016/j.foodhyd.2023.109657

Li, C., & Gong, B. (2020). Insights into chain-length distributions of amylopectin and amylose molecules on the gelatinization property of rice starches. *International Journal of Biological Macromolecules, 155*, 721–729. https://doi.org/10.1016/j.ijbiomac.2020.04.006

Li, E., Cao, P., Cao, W., & Li, C. (2022). Relations between starch fine molecular structures with gelatinization property under different moisture content. *Carbohydrate Polymers, 278*, Article 118955. https://doi.org/10.1016/j.carbpol.2021.118955

Li, Z., Wang, L., Chen, Z., Yu, Q., & Feng, W. (2018). Impact of protein content on processing and texture properties of waxy rice flour and glutinous dumpling. *Journal of Cereal Science, 81*, 30–36. https://doi.org/10.1016/j.jcs.2018.03.005

Lin, L., Guo, K., Zhang, L., Zhang, C., Liu, Q., & Wei, C. (2019). Effects of molecular compositions on crystalline structure and functional properties of rice starches with different amylopectin extra-long chains. *Food Hydrocolloids, 88*, 137–145. https://doi.org/10.1016/j.foodhyd.2018.09.033

Lin, Z., Geng, D. H., Qin, W., Huang, J., Wang, L., Liu, L., & Tong, L. T. (2021). Effects of damaged starch on glutinous rice flour properties and sweet dumpling qualities. *International Journal of Biological Macromolecules, 181*, 390–397. https://doi.org/10.1016/j.ijbiomac.2021.03.160

Miao, M., Jiang, B., Cui, S. W., Zhang, T., & Jin, Z. (2015). Slowly digestible starch—A review. *Critical Reviews in Food Science and Nutrition, 55*(12), 1642–1657. https://doi.org/10.1080/10408398.2012.704434

Phongthai, S., D'Amico, S., Schoenlechner, R., Homthawornchoo, W., & Rawdkuen, S. (2017). Effects of protein enrichment on the properties of rice flour based gluten-free pasta. *Lwt, 80*, 378–385. https://doi.org/10.1016/j.lwt.2017.02.044

Rostamabadi, H., Bajer, D., Demirkesen, I., Kumar, Y., Su, C., Wang, Y., … Falsafi, S. R. (2023). Starch modification through its combination with other molecules: Gums, mucilages, polyphenols and salts. *Carbohydrate Polymers, 314*, Article 120905. https://doi.org/10.1016/j.carbpol.2023.120905

Sasaki, T., Kohyama, K., Suzuki, Y., Okamoto, K., Noel, T. R., & Ring, S. G. (2009). Physicochemical characteristics of waxy rice starch influencing the in vitro digestibility of a starch gel. *Food Chemistry, 116*(1), 137–142.

Singh, N., Kaur, L., Sandhu, K. S., Kaur, J., & Nishinari, K. (2006). Relationships between physicochemical, morphological, thermal, rheological properties of rice starches. *Food Hydrocolloids, 20*(4), 532–542. https://doi.org/10.1016/j.foodhyd.2005.05.003

Sun, Y., Li, F., Luan, Y., Li, P., Dong, X., Chen, M., Dai, L., & Sun, Q. (2021). Gelatinization, pasting, and rheological properties of pea starch in alcohol solution. *Food Hydrocolloids, 112*, Article 106331. https://doi.org/10.1016/j.foodhyd.2020.106331

Tao, K., Yu, W., Prakash, S., & Gilbert, R. G. (2019). High-amylose rice: Starch molecular structural features controlling cooked rice texture and preference. *Carbohydrate Polymers, 219*, 251–260. https://doi.org/10.1016/j.carbpol.2019.05.031

Wang, H., Xiao, N., Wang, X., Zhao, X., & Zhang, H. (2019). Effect of pregelatinized starch on the characteristics, microstructures, and quality attributes of glutinous rice flour and dumplings. *Food Chemistry, 283*, 248–256. https://doi.org/10.1016/j.foodchem.2019.01.047

Wang, S., Li, P., Yu, J., Guo, P., & Wang, S. (2017). Multi-scale structures and functional properties of starches from Indica hybrid, japonica and waxy rice. *International Journal of Biological Macromolecules, 102*, 136–143. https://doi.org/10.1016/j.ijbiomac.2017.04.020

Yi, C., Zhu, H., Bao, J., Quan, K., & Yang, R. (2020). The texture of fresh rice noodles as affected by the physicochemical properties and starch fine structure of aged paddy. *Lwt, 130*, Article 109610. https://doi.org/10.1016/j.lwt.2020.109610

You, S. Y., Lim, S. T., Lee, J. H., & Chung, H. J. (2014). Impact of molecular and crystalline structures on in vitro digestibility of waxy rice starches. *Carbohydrate Polymers, 112*, 729–735. https://doi.org/10.1016/j.carbpol.2014.06.065

Yousefi, A. R., & Razavi, S. M. (2015). Dynamic rheological properties of wheat starch gels as affected by chemical modification and concentration. *Starch-Stärke, 67*(7–8), 567–576. https://doi.org/10.1002/star.201500005

Zhang, Z., Wang, Y., Ling, J., Yang, R., Zhu, L., & Zhao, W. (2022). Radio frequency treatment improved the slowly digestive characteristics of rice flour. *Lwt, 154*, Article 112862. https://doi.org/10.1016/j.lwt.2021.112862

Zheng, F., Xu, Q., Zeng, S., Zhao, Z., Xing, Y., Chen, J., & Zhang, P. (2023). Multi-scale structural characteristics of black Tartary buckwheat resistant starch by autoclaving combined with debranching modification. *International Journal of Biological Macromolecules, 249*, Article 126102. https://doi.org/10.1016/j.ijbiomac.2023.126102

Zhou, W., Yang, J., Hong, Y., Liu, G., Zheng, J., Gu, Z., & Zhang, P. (2015). Impact of amylose content on starch physicochemical properties in transgenic sweet potato. *Carbohydrate Polymers, 122*, 417–427. https://doi.org/10.1016/j.carbpol.2014.11.003

Zhu, L., Zhang, Y., Wu, G., Qi, X., Dag, D., Kong, F., & Zhang, H. (2020). Characteristics of pasting properties and morphology changes of rice starch and flour under different heating modes. *International Journal of Biological Macromolecules, 149*, 246–255. https://doi.org/10.1016/j.ijbiomac.2020.01.161